DOUBLE TUNING OF A DUAL EXTERNAL CAVITY SEMICONDUCTOR LASER FOR BROAD WAVELENGTH TUNING WITH HIGH SIDE MODE SUPPRESSION

DOUBLE TUNING OF A DUAL EXTERNAL CAVITY SEMICONDUCTOR LASER FOR BROAD WAVELENGTH TUNING WITH HIGH SIDE MODE SUPPRESSION

By

Ali M. Abu-El-Magd

Bachelor's of Engineering

McMaster University, June 2005

A THESIS

SUBMITTED TO THE SCHOOL OF GRADUATE STUDIES IN PARTIAL FULFILLMENT OF THE REQUIREMENTS FOR THE DEGREE OF MASTER'S OF APPLIED SCIENCE

McMaster University

Hamilton, Ontario, Canada

MASTER OF APPLIED SCIENCE (2011)	McMaster University
(Electrical and Computer Engineering)	Hamilton, Ontario

TITLE:	Double Tuning Of A Dual External Cavity Semiconductor Laser For Broad Wavelength Tuning With High Side Mode Suppression
AUTHOR:	Ali M. Abu-El-Magd, B.Eng. (McMaster University)
SUPERVISORS:	Prof. R.N. Kleiman and Dr. Y.M. Haddara
NUMBER OF PAGES:	xii, 65

Abstract

Over the past few years various successful miniaturization attempts of External Cavity Semiconductor Lasers (ECSL) were published. They built upon the rich literature of ECSL configurations that were extensively analyzed and improved upon since the 1960s. This was merged with the microfabrication techniques of 3D structures based on MEMS technology. The main drive for miniaturizing such tunable lasers in the recent past was the huge potential for such devices in all optical networks specifically as signal sources that enable Wavelength Division Multiplexing (WDM).

This thesis compares the different configurations chosen to build tunable lasers using MOEMS technology. Our criteria of comparison include wavelength tuning range, side mode suppression, tuning speed and device dimensions. Designs based on the simple ECSL with a movable external mirror suffered from the tradeoff between tuning range and Side Mode Suppression SMS. To overcome this limitation most designs adopted grating based tuning using the Littrow or Littman/Metcalf configurations. These configurations allow for much better tuning results but don't lend themselves easily to miniaturization. The grating based devices were bulky and quite complicated to realize.

We propose the adoption of the Zhu/Cassidy double external cavity configuration. It retains the simplicity of the single external mirror configuration along with the tuning range and the SMS of including multiple tuning elements. In its original form this configuration suffered from mode hopping within the tuning range. Thorough simulation, design and experimental evidence is presented in this work to show that by extending the configuration to allow full control over both optical tuning elements this drawback can be eliminated.

Our proposed design would reduce the form factor to < 300µm x 200µm x 200µm. The voltage required to tune through all the modes is < 40V and the resonant frequency of the mirror is in the 10s of MHz order of magnitude. When coupled with a multimode laser of

a sufficiently broad lasing profile this setup should enable a tuning range > 72nm with a SMS >20dB.

Acknowledgements

In the name of God the most gracious, the most merciful. By His will, I have produced and documented this work. While all gratitude and praise belongs to Him, it is also true that “He who does not acknowledge and credit God’s creation does not, by association, pay proper gratitude to the Almighty.”

With this in mind, I would like to express my deepest gratitude to Professor R.N. Kleiman, my principal supervisor, for giving me the opportunity to work on this project as well as his continued support and guidance. It was an honour to have been one of his students.

I would also like to express my sincere appreciation to my co-supervisor and older brother Dr. Y.M. Haddara for his guidance and support along the course of my master’s program. His continued commitment in motivating me to complete and document my work has been crucial. Furthermore, beyond the academic realm, he is also a great inspiration for me in my community involvement and personal development. I feel very privileged to have his presence in my life.

A special thank-you is in order to Professor D.T. Cassidy for allowing me to conduct my experiments in his lab, as well as his research group for treating me as one of their own. Within that research group I would like to specifically single out Dr. Hesham Enshasy and acknowledge his enormous help in setting up my experiments. His contributions were invaluable to me, in particular for optical alignment and for wire bonding to the lasers.

I would also like to thank the “Natural Sciences and Engineering Research Council of Canada” (NSERC) and the “Ministry of Training Colleges and Universities” of the province of Ontario for funding my research.

Very special thanks go to my dear friend, Dr. Munir El-Desouki, for providing me with a thesis template to eliminate one of my many excuses to not complete my degree.

My sincere appreciation is due to my defense committee members, Dr. A. Jeremic and Dr. S. Dumitrescu, for their constructive remarks and helpful corrections.

It took me four years to write up my thesis and it would have been impossible to find the motivation if it weren't for my parents, Professor M. Abu-El-Magd and Professor Z. Ashour, and their continued persistence. It wouldn't have been possible as well without my loving wife Ayah and our beloved newborn Ibraheem. His arrival to this world, a few months before writing these lines, was my biggest joy and inspiration.

Table of Contents

List of Figures

List of Tables

List of Acronyms

AFCRL	Air Force Cambridge Research Laboratories
AR	Anti-Reflective
BSOI	Bonded Silicon on Insulator
DBR	Distributed Brag Reflector
DFB	Distributed Feedback
DMD	Digital Micromirror Devices
DRIE	Deep Reactive Ion Etching
DWDM	Dense Wavelength Division Multiplexing
ECSL	External Cavity Semiconductor Laser
FP	Fabry-Perot
GPIB	General Purpose Interface Bus
HITRAN	High-resolution Transmission Molecular Absorption Database
HR	Half Reflective
MBE	Molecular Beam Epitaxy
MEMS	Micro-Electro-Mechanical Systems
MOEMS	Micro-Opto-Electro-Mechanical Systems
OSA	Optical Spectrum Analyzer
PSG	Phosphosilicate Glass
RIE	Reactive Ion Etching
SFB	Silicon Fusion Bonding
SMSR	Side Mode Suppression Ratio
SOA	Semiconductor Optical Amplifiers
SOI	Silicon on Insulator
VI	Virtual Instrument
WDM	Wavelength Division Multiplexing

Chapter 1

INTRODUCTION

1.1 Tunable Lasers

Tunable external cavity semiconductor lasers (ECSL) have been long considered a slow wavelength tuning option with good spectral characteristics in comparison to the alternative distributed-Brag-reflector (DBR), distributed feedback (DFB) and vertical cavity surface-emitting lasers (VCSEL). The main reason for the considerably low tuning speed is the need for a mechanical movement to realize the tuning. Recent efforts [1-3] have been demonstrated in an attempt to miniaturize ECSL using micro-opto-electro-mechanical system (MOEMS) design techniques. MOEMS electrostatic actuation techniques not only enable higher tuning speeds, but they also promise to reduce production costs and enable a set of applications that could have only been made possible on the micro level.

1.1.1 Applications

Tunable ECSLs have multiple applications in the fields of optical coherent telecommunications, sensing and precise measurements [4]. An appealing use for tunable ECSLs in optical telecommunications is in wavelength division multiplexing (WDM). Multiple channels at different frequencies utilizing the same fiber cable and traveling across long distances would typically require intermediate optical add/drop ports for signal amplification and channel control. A tunable ECSL can serve as a configurable transmitter source to enable the addition of one or multiple channels. On the other hand a tunable filter element would selectively remove channels [5].

Detecting environmentally unfriendly gases such as carbon monoxide, sulfur dioxide, methane, formaldehyde and nitrous oxide and monitoring their concentrations is important for air quality control in spacecraft and medical environments, leakage detection at plants and factories, non-invasive medical diagnostics as well as many other environmental applications.

Laser absorption spectroscopy is considered an effective technique for gas detection. This method relies primarily on exciting the gas molecules with a range of frequencies and detecting those specific frequencies at which orbital transitions occur. These absorbed frequencies indicate the identity of the studied gas.

Values used in spectral calculations such as absorption wavelengths, line strengths, line center, wave numbers, linewidths and pressure broadening parameters for atmospheric molecules can be obtained by researchers from the High-resolution Transmission Molecular Absorption Database (HITRAN) [6]. This database was a project started in the Air Force Cambridge Research Laboratories (AFCRL) and is now carried on in Harvard University.

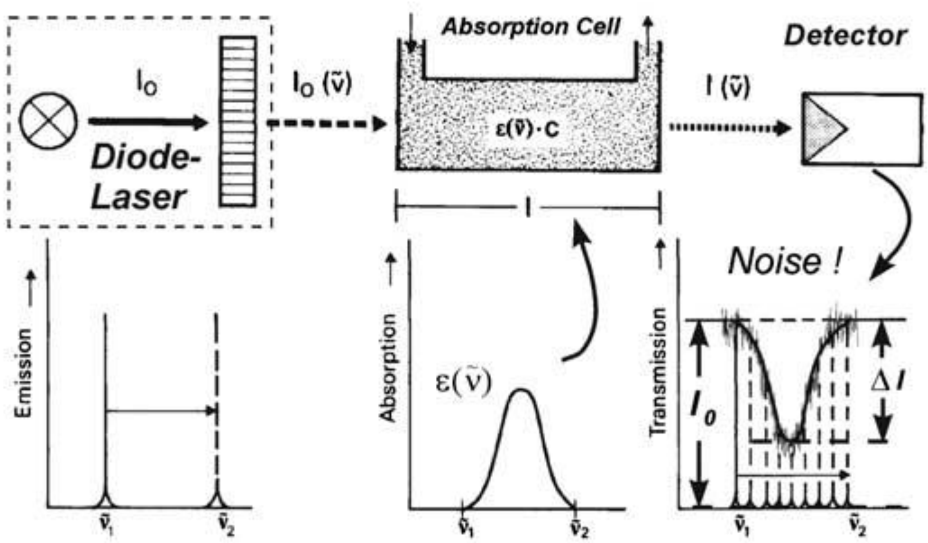

Figure 1.1: Laser Absorption Spectroscopy [7]

A standard detection system is shown in figure 1.1 [7]. The schematic indicates how a tunable diode laser sweeps the desired frequency range for detection. This laser is aligned with a cell containing the material to be detected. A detector is then used to calculate the absorption spectrum of the material giving away its nature by comparing with HITRAN values.

1.2 Tunable External Cavity Semiconductor Lasers (ECSL)

1.2.1 Theory

Tuning Principles

Induced emissions in semiconductor devices are band-based rather than atomic state transitions. This results in a wider gain profile with respect to frequency. Despite this being viewed as a downside in standard laser design, it turns out to be quite useful when it comes to tunable lasers. If the gain medium already induces emission in a wide range of frequencies, then it is possible by an externally controlled filtering mechanism to select the desired output frequency. This is the primary principle of designing and operating an ECSL. The general tuning idea and the basic configuration can be viewed in figure 1.2 and is also summarized in the following relation [5].

$$\frac{\Delta\lambda}{\lambda} = \frac{\Delta n}{n} + \frac{\Delta L}{L} - \frac{\Delta m}{m} \tag{1.1}$$

λ is the output wavelength, n is the effective cavity length and m is the resonance mode of the cavity.

Effective Reflectivity Concept

The effect of changing the length of the external cavity of the laser can be understood from the effective reflectivity model. In a standard single cavity laser system the loss induced by the resonant cavity's reflectors is described by the following relation.

$$\alpha = \frac{1}{d} \ln \frac{1}{r_1 r_2} \tag{1.2}$$

d is the primary cavity's length and r_1 and r_2 are the reflectivities of its left and right facets respectively.

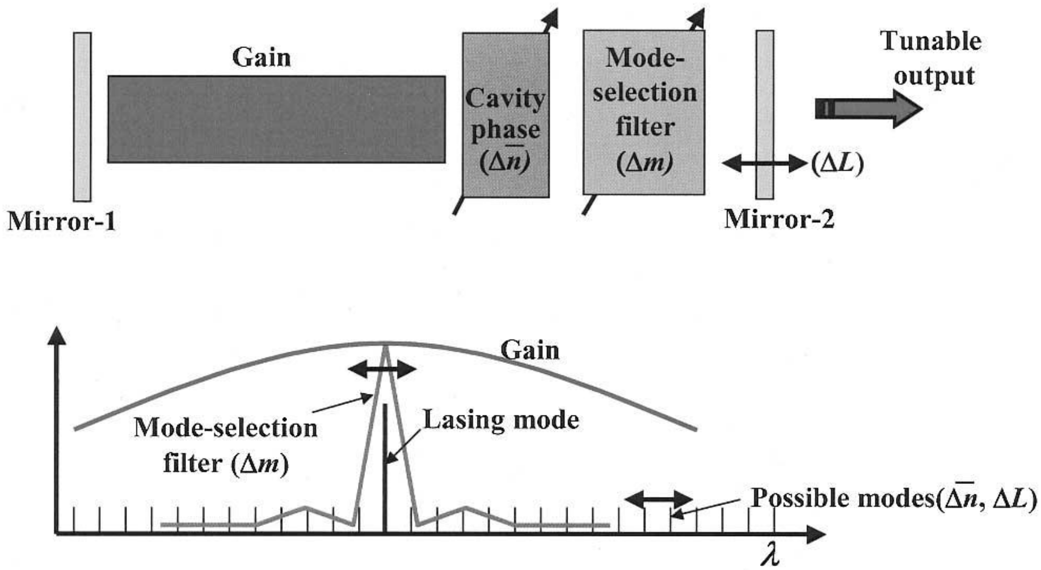

Figure 1.2: ECSL Tuning Principles [5]

Assuming r_1 and r_2 are constant over the operating range of frequencies, the loss profile is constant over all frequencies. In the case of an ECSL we can incorporate the coupling between both cavities, the delay in the external cavity and the reflectivity of the external mirror into a complex effective reflectivity. The system thus reduces to a single cavity system and can be treated accordingly [8-10].

$$R_{\mathrm{eff}}(\lambda) = \frac{r_2 + r_3 \exp(-j4\pi n L_c/\lambda)}{1 + r_2 r_3 \exp(-j4\pi n L_c/\lambda)} \tag{1.3}$$

where r_3 is the external mirror's reflectivity.

$$\alpha(\lambda) = \frac{1}{d} \ln \frac{1}{r_1 \mid R_{\mathrm{eff}}(\lambda) \mid} \tag{1.4}$$

The loss profile is in this case frequency dependent, which provides a filtering factor controlled by the external cavity's length. We can calculate the suppression of a laser mode with respect to the main mode by finding the difference in their loss to yield the following result.

$$\Delta\alpha = \frac{1}{d} \ln \frac{\mid R_{\mathrm{eff}}(\lambda_0) \mid}{\mid R_{\mathrm{eff}}(\lambda_i) \mid} \tag{1.5}$$

where λ_0 and λ_i are two competing wavelengths that coincide with resonant modes of the cavity.

Grating-based Tuning

The competition of laser modes in simple ECSL configurations is not completely resolved from the loss profile. It is a delicate design issue finding the external cavity length ranges where the side mode suppression is at its maximum. This led to the idea of replacing the external cavity's mirror with a blazed grating.

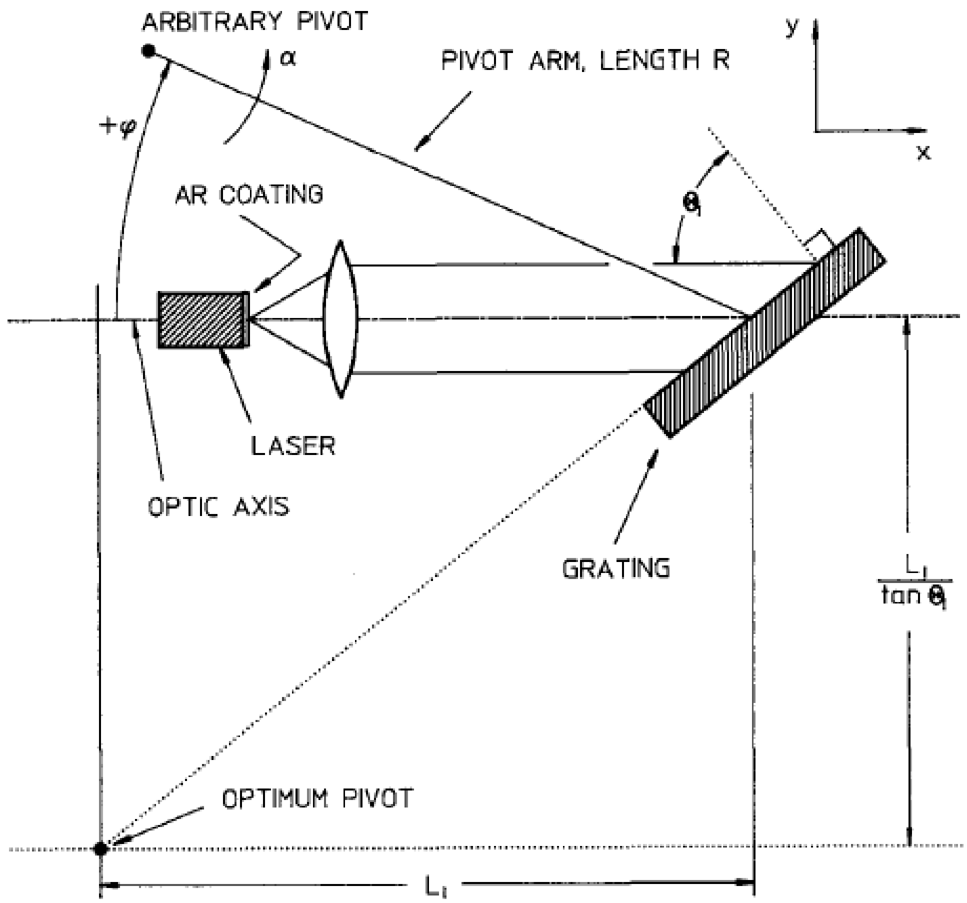

Figure 1.3: Grating Based Tuning (Littrow Configuration) [11]

The grating acts as a fine tune filter to select only the desired frequency. It is then a matter of matching the grating's selected frequency given by [11]

$$\nu_g = \frac{c}{2\mathrm{dsin}\theta} \tag{1.6}$$

to one of the cavity's resonant modes, which are spaced according to

$$\Delta\nu_{\mathrm{mode}} = \frac{c}{2\mathrm{L}} \tag{1.7}$$

Tracking a specific cavity mode with the grating guarantees continuous wavelength tuning. This can only be achieved by changing the displacement of the mirror and the rotation angle of the grating at a fixed pace. A simple approximation for achieving that involves using a fixed pivot point and rotating the mirror about it. The ideal pivot point in a Littrow configuration (shown in figure 1.3) is described by [11]

$$R = \frac{L_i}{\sin\theta_i} \tag{1.8}$$

$$\text{and } \Phi = \theta_i - 90° \tag{1.9}$$

where R and Φrepresent the optimal pivot point's arm length and angle when the initial external cavity length and grating angle are L_i and θ_i.

1.3 Tunable MOEMS ECSL Review

1.3.1 Design Techniques

Standing Structures

Conventional MEMS mirrors are those used in digital micromirror devices (DMD). They rotate by electrostatic control about a fixed axis allowing a tilting motion for the mirror structure [12], [13]. In the case of an ECSL it is required to design a mirror with the ability to translate with the aid of an actuator. One way of achieving this requirement is by fabricating a mirror that would flip out of the substrate and stand vertically on top of the substrate. Releasing the standing structure and aligning the mirror to maintain accurate positioning is a major design challenge.

In 2001 Vaccaro et al. [14] proposed a self-positioning method based on the lattice mismatch of epitaxially grown layers. They used molecular beam epitaxy (MBE) to deposit two layers with a mismatch in their lattice constants to serve as a hinge for the mirror. The lower layer has a larger lattice constant than that of the upper layer. When released both layers bend upwards to relax the strain and the curvature of bending [15] depends on the lattice constants of the material, the ratio in Young moduli and the ratio of the deposited layer thicknesses. Figure 1.4 [14] illustrates a microfabrication process of a vertical mirror using their strain induced self-alignment technique. This technique was never applied to an ECSL design, despite it being simple and very flexible.

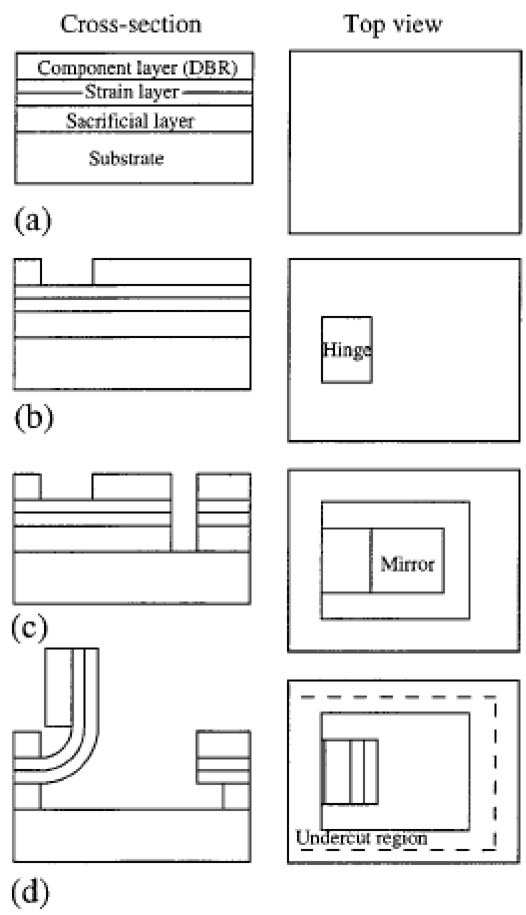

Figure 1.4: Strain Induced Self-Alignment (Vertical Structure Microfabrication Technique) [14]

A more commonly used approach to create standing mirrors is by depositing layers that serve as hinges for the standing structure. Figure 1.5 [16] shows a basic version of the process. A sacrificial layer of phosphosilicate glass (PSG) is first deposited on the substrate. It is followed by the deposition and patterning of a polysilicon layer which represents the structure of the mirror. Another PSG layer is then deposited followed by the etching of contacts for the hinge through both PSG layers. A second polysilicon layer is then deposited and patterned to form the hinge of the mirror. In the end the sacrificial PSG layers are selectively etched to release the mirror structure. Figure 1.6 shows an ECSL fabricated in a similar fashion [1].

This process however is incomplete until the mirrors are lifted off from the surface of the substrate to the required position. The standard way of doing this involves the use of microprobes. While this might be acceptable in a research lab, it is quite inefficient, slow and costly in an industrial process. Automated MEMS assembly systems can be designed on the same substrate to lift off the structures to their required positions [17]. This is achieved by use of vertical actuators.

Deep Reactive Ion Etching (DRIE)

Vertical etching techniques of silicon substrates have undergone significant progress. Older wet etching techniques were based on the difference in etching rates of some chemical etchants to silicon in different directions. One such etchant is KOH, which etches at a much faster rate in the [100] direction than in the [111] direction [18]. In general however wet etching is considered an isotropic process.

The more commonly used plasma etching systems make it easier to achieve vertical etching. In plasma etching several mechanisms are involved in the process [15]. While some isotropic chemical etching is still involved, reactive neutral species and ionic species are also involved in the process. The etching achieved from ionic species is completely anisotropic, but lacks selectivity. There are two [15] main reasons that make selectivity a vital issue:

⇒ We are protecting the remainder of our substrate with a mask layer. It is also subject to the bombardment of the ionic species. As we etch deeper in the substrate our mask layer might be also etched through, revealing undesired regions for etching.

There is some uncertainty associated with the thickness of the etched layer. To overcome this uncertainty an amount of overetching is inevitable. Non selectivity of the process could result in some etching of the layer underneath.

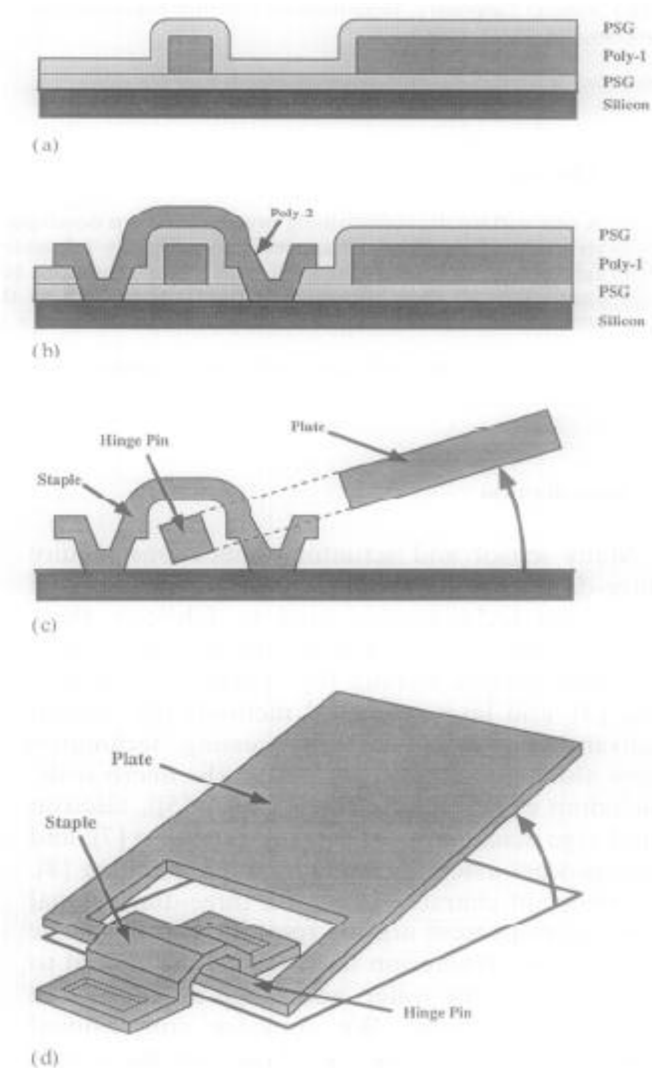

Figure 1.5: Hinged Vertical Mirror Microfabrication Process [16]

The more commonly used plasma etching systems make it easier to achieve vertical etching. In plasma etching several mechanisms are involved in the process [15]. While some isotropic chemical etching is still involved, reactive neutral species and ionic species are also involved in the process. The etching achieved from ionic species is completely anisotropic, but lacks selectivity.

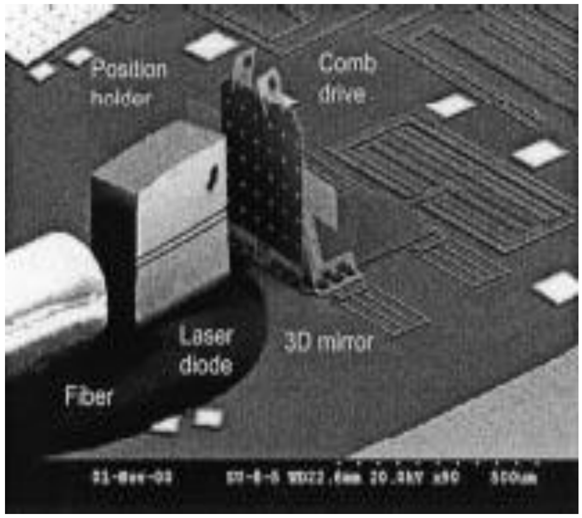

Figure 1.6:ECSL With A Hinged Mirror [21]

There are two [15] main reasons that make selectivity a vital issue:

⇒ We are protecting the remainder of our substrate with a mask layer. It is also subject to the bombardment of the ionic species. As we etch deeper in the substrate our mask layer might be also etched through, revealing undesired regions for etching.

⇒ There is some uncertainty associated with the thickness of the etched layer. To overcome this uncertainty an amount of overetching is inevitable. Non selectivity of the process could result in some etching of the layer underneath.

Reactive ion etching (RIE) and DRIE systems rely on ion enhanced etching, where a combination of ions and reactive neutral species are used in the etching process. This method maintains the anisotropic stature of the physical ionic bombardment process and introduces a fair amount of selectivity [15].

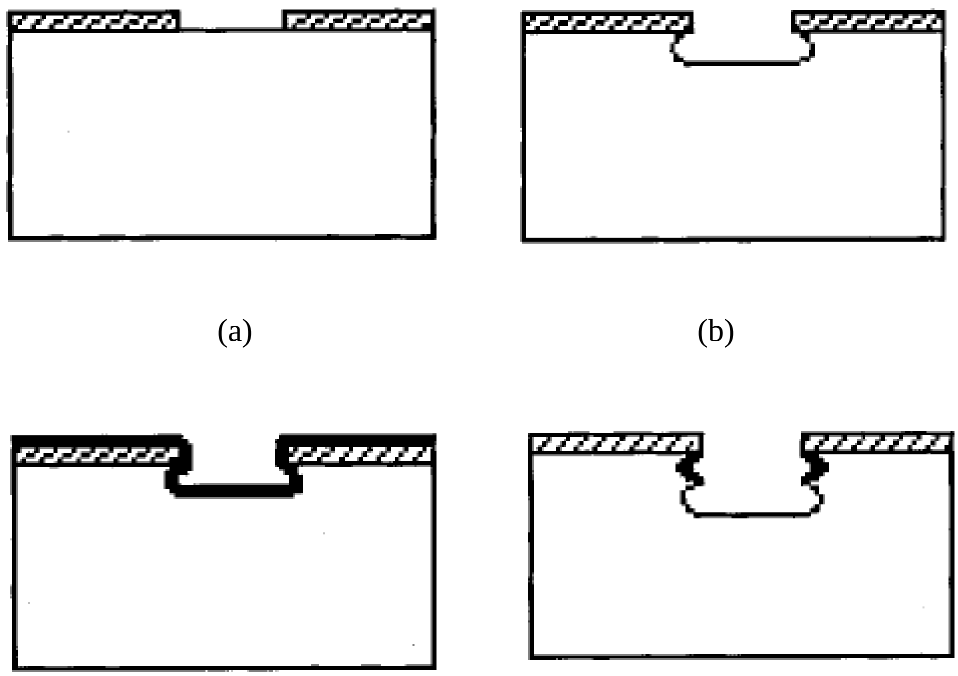

(a) (b)

(c) (d)

Figure 1.7: Deep Reactive Ion Etching Process Steps [19]

Robert Bosch enhanced RIE using an approach illustrated in figure 1.7 patented as DRIE [19]. The point was to prevent any isotropic etching effects from occurring due to the reactive neutral species. These effects start to show when regular RIE is used for very deep structures. Bosch’s approach [19] is based on a cycle of two steps. The wafer is first etched in a manner identical to RIE with SF_6 as gas. C_4F_8 is then used to passivate the groove with a fluorocarbon film. In the etching part of the following cycle neutral species are prevented from reacting with the side walls of the structure, but ion bombardment will etch through the bottom layer and further in the substrate providing highly anisotropic etching.

After creating a structure using DRIE it needs to be released for mechanical movement. Silicon fusion bonding (SFB) can be used to enable this step. Figure 1.8 shows how DRIE and SFB can be combined to fabricate MEMS and MOEMS structures [19]. Two wafers are involved in the process. The bottom wafer is first etched before it is fusion bonded to a regular top wafer. A hollow cavity is now present inside the bonded wafer. Vertical structures are then etched in the wafer using DRIE. When the DRIE reaches the buried cavity the structures become automatically released.

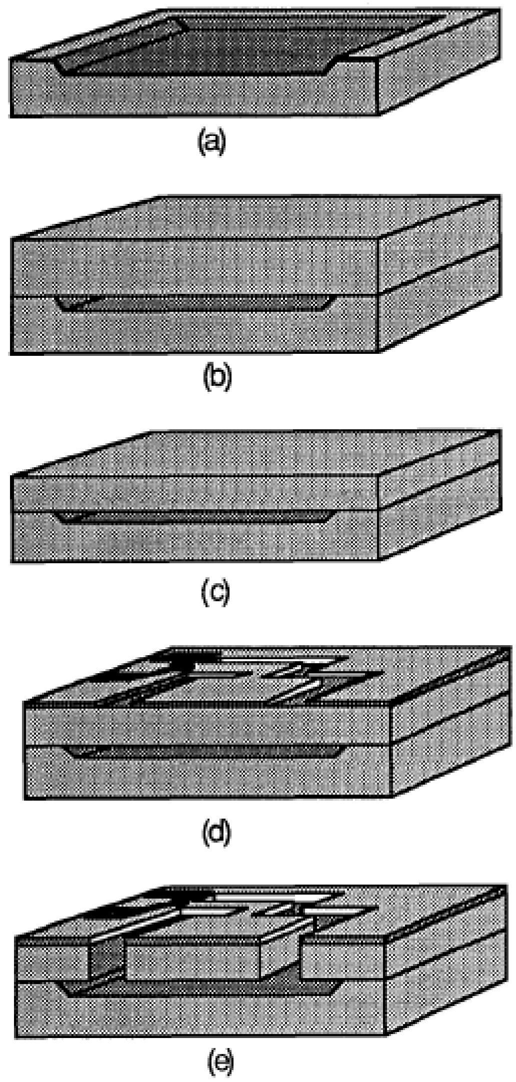

Figure 1.8: SFB Fabrication Process Steps [3]

The last step involved in obtaining our vertical mirror involves controlling its reflectivity. Thin films with thicknesses of 40-60nm of aluminum or gold [20] are deposited on the desired surface to enhance the reflectivity of the mirror.

Mirrors fabricated using DRIE and SFB techniques allow for better integration with the actuation system. They help achieve finer tuning steps and faster tuning rates. The combination of DRIE and SFB is also used in fabricating the actuator. Figure 1.11 shows a complete ECSL system where both the combdrive actuator and the curved mirror were realized by DRIE [3].

1.3.2 Device Designs

The potential that a miniature tunable laser has in DWDM networks as described in the first chapter of this work coupled with the performance that previous non-microscale designs have demonstrated have tempted many MEMS research groups in the recent past to attempt to design miniature tunable ECSL. Using some of the techniques presented in the previous section yielded various degrees of success in obtaining the desired results. It is important to point out that the objectives of designing a tunable MEMS device was to guarantee shrinking the system and an enhancement in the tuning speed of the laser, while attempting to maintain the performance obtained by the classical ECSL designs using the same geometries.

1-D Designs

By one dimensional designs we are referring to the very basic ECSL geometry with a standard FP semiconductor laser coupled on one end with a highly reflective movable mirror and the output of the laser is collected from the other end. The length of the gap between the laser and the external mirror is varied by means of a linear actuator attached to the mirror.

As was described earlier in section 1.3.1 a mirror can be surface machined on the wafer and made to rotate about a hinge when released to stand vertically on the wafer. Shown above in figure 1.9 is the attempt [21] made by the research group at Nanyang Technological University in Singapore, where a combdrive was fabricated attached to the mirror to act as the linear actuator for the system. The laser was later stuck to the surface of the wafer in front of the released standing mirror and coupled to an optical fiber from the other side. A continuous tuning range of 16nm was achieved as the external cavity length was varied from 10µm to 11µm as shown in figure 1.10. The single mode outputs had a side mode suppression ratio (SMSR) greater than 30dB.

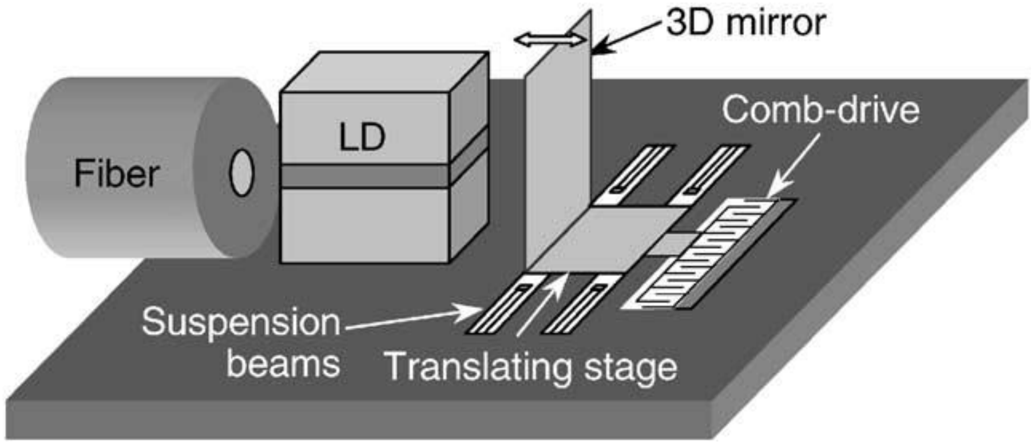

Figure 1.9: 1D ECSL with Pop-Up Mirror (NTU) [21]

Despite the successful usage of MEMS technology to create a vertical reflective element coupled with a linear actuator the fruits of miniaturization were not yet reaped in this early design. The hinged standing mirror structure needed to be manually released using microprobes limiting this design to lab usage. The overall dimensions of the device, because of its hybrid nature were as big as 2mmx1.5mmx1mm which is an enhancement to non-MEMS actuator based devices that share the laser and the mirror dimensions and use a larger piezoelectric mirror for actuation. On the positive side the actuator's driving voltage was as low as 10V and was only varied in a 6V range to tune the laser through all possible modes. However, the tuning speed was not reported. And even though combdrives can usually move at high speeds, the size and design of this structure would dictate slower movement. Overall this attempt has only successfully leveraged MEMS techniques to reduce the size of the actuator and use lower voltage bias for it.

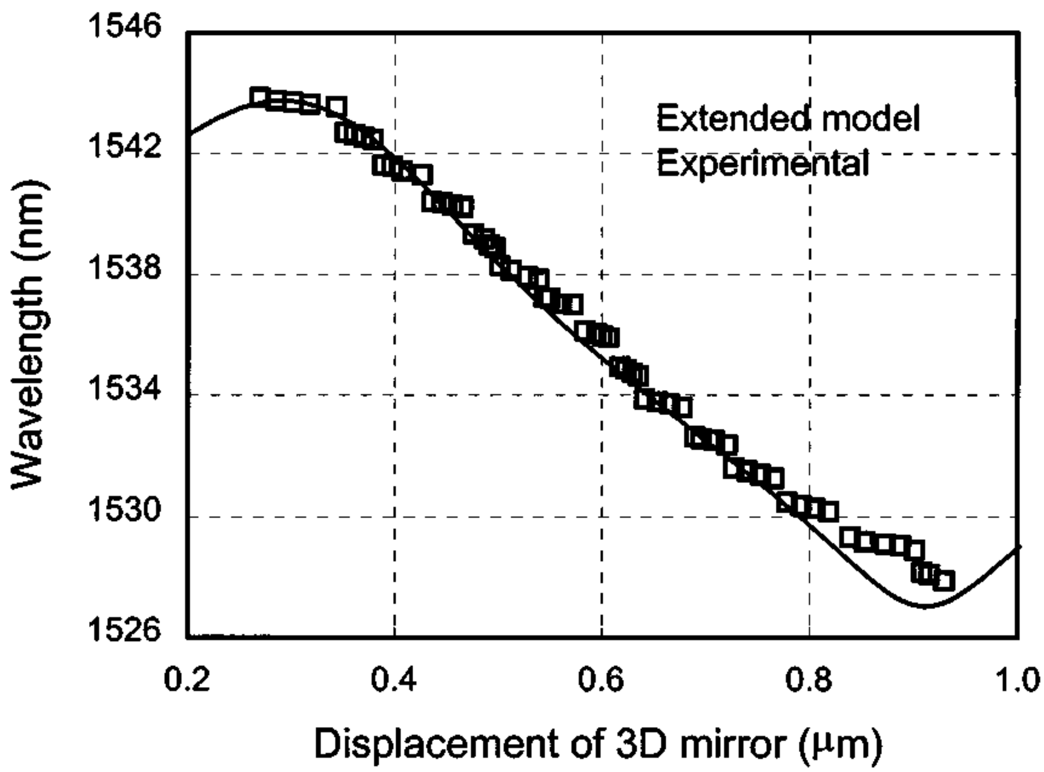

Figure 1.10: Tuning Profile of System Shown in Figure 1.9 (NTU) [21]

A later attempt [22] made by the same group at Nanyang took the design one level further. Shown in figure 1.11 is an SEM of their ECSL system. This time around DRIE was adapted in the fabrication process of the device in a silicon on insulator (SOI) wafer to realize both the actuator and the mirror. A combdrive was also designed for actuation purposes attached to a curved mirror vertically etched into the substrate. A cavity was also etched out for the laser to be placed and aligned against the mirror. A fiber again was positioned on the other side of the laser to collect the output. A continuous tuning range of 13.5nm was repeatedly obtained as the external mirror was displaced varying the external cavity length from 66μm to 70μm as shown in figure 1.12. The SMSR of all output frequencies was greater than 13dB.

This design is definitely one step ahead of the former. Having the actuator and the attached mirror fabricated part of one rigid structure has several advantages. It reduced the amount of components occupying space in the dimension perpendicular to the substrate. This can be observed from the reported dimensions of the device 1.5mmx1mmx0.6mm. It also allowed for faster tuning speeds. The reported resonant frequency of the combined structure of the combdrive and the mirror is 2.5kHz. It was also claimed that a switch from one mode to any other could be done in less than 1ms. A relatively small driving voltage for the actuator movement was maintained in this design as well. The 4µm movement was driven by a 2.5 to 18V variation.

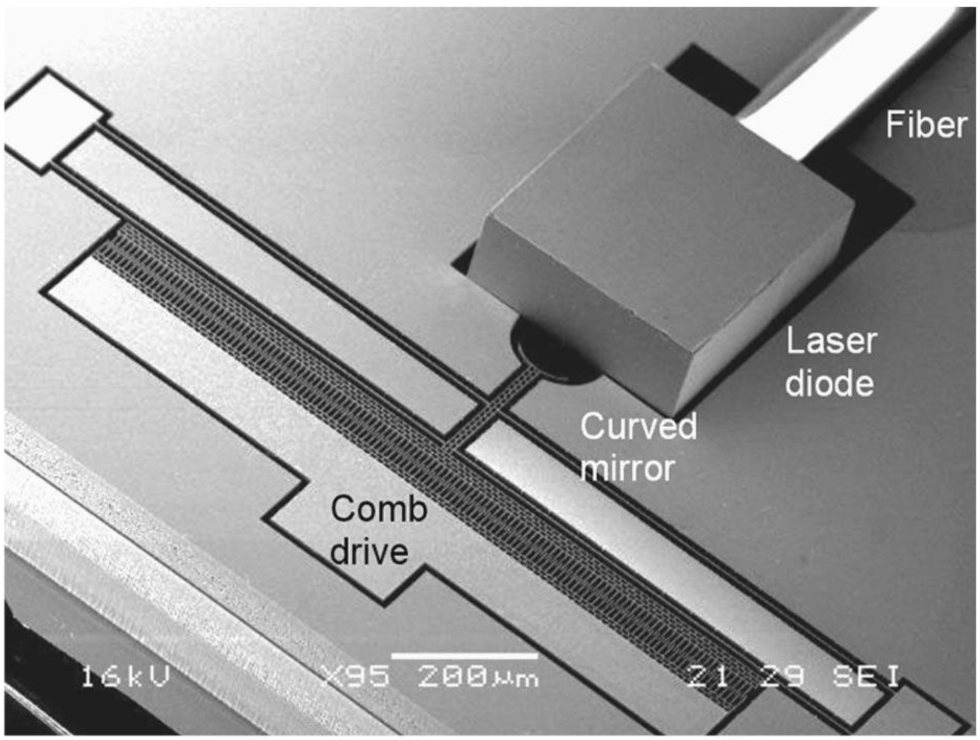

Figure 1.11: 1D ECSL Using DRIE (NTU) [22]

Littrow Designs

As was the case with conventional ECSL more complex geometries were used to allow for an extended tuning range while maintaining good side mode suppression. Figure 1.13 shows the setup [23] by the research group at Imperial College London. For this setup they used DRIE of bonded SOI to fabricate the moving part of the device; namely the grating and the attached actuation mechanism. The rest of the components were off chip.

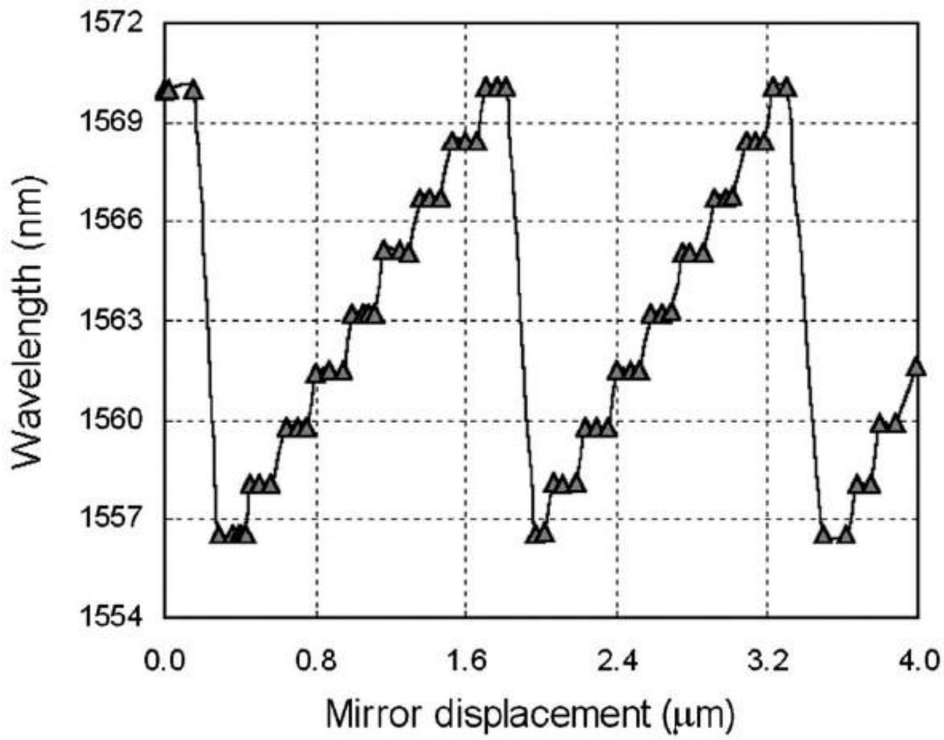

Figure 1.12: Tuning Profile of System Shown in Figure 1.11 (NTU) [22]

The actuation mechanism consisted of two linear combdrives to mimic a rotational movement. One drive moves the cantilever arm tangentially about the desired pivot point, while the other independently moves the mirror linearly to have control over the external cavity length. This control will allow for corrections to the deviation in imitating a real rotational movement by the first actuator. A tuning range of 20nm with a SMSR greater than 20dB was obtained using this design.

The complexity of the geometry has to be taken into consideration. However, everything about that setup was bulky. The size of the device was not reported, but several dimensions could serve as good indicators. A pivot arm length of 2mm was fabricated to maintain the Littrow configuration conditions for continuous tuning. And the external cavity length was reported to be 1.63mm. The speed of tuning was also not reported, but 14µm of movement were needed to cover the tuning range. Those were driven by a supply within 50V.

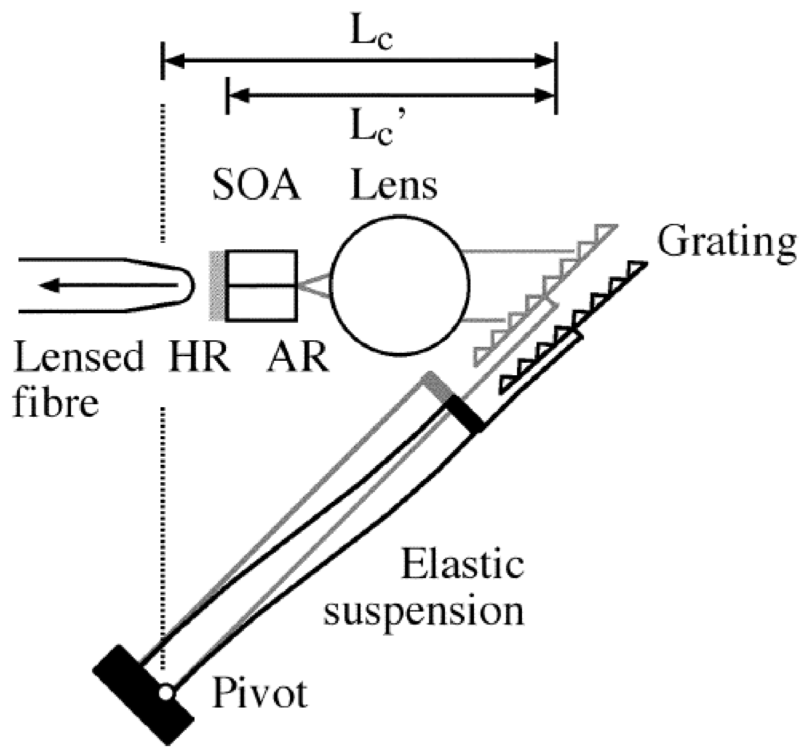

Figure 1.13: Littrow ECSL Setup Using Elastic Suspension (ICL) [23]

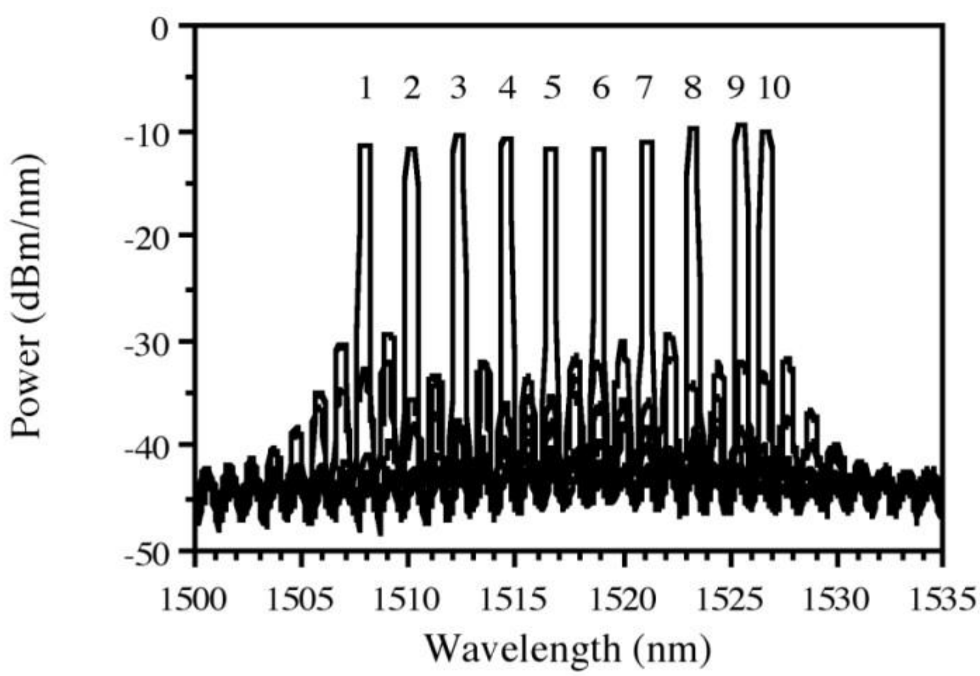

Figure 1.14: Tuning Profile of System Shown in Figure 1.13 (ICL) [23]

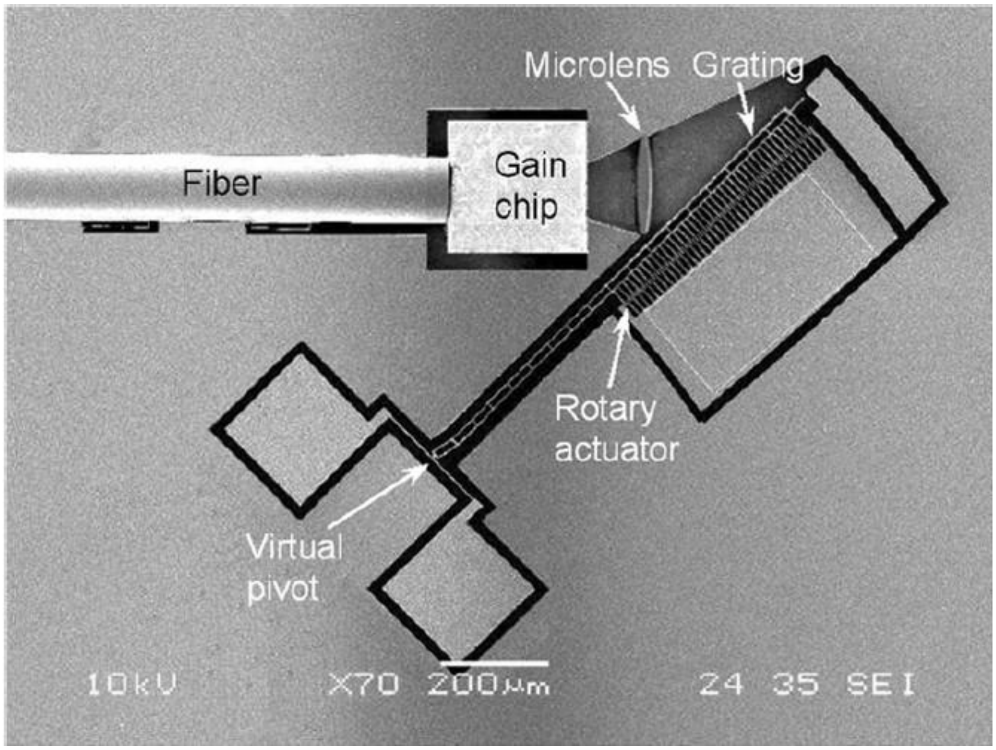

Figure 1.15: Littrow ECSL Setup Using Rotary Combdrive (NTU) [24]

Another attempt [24] at a MOEMS Littrow configuration was done by the group at Nanyang. Shown in figure 1.15 is their setup, which differs from the Imperial setup by the presence of the laser and the lens on chip. DRIE was used to etch grooves to place those components in the same substrate containing the MEMS actuator structure. The other difference is the construction of a rotary combdrive actuator. 30.3nm of continuous tuning was reported with a SMSR that ranged from 12 to 26dB.

This attempt showed some improvements that are mostly related to having everything on the same chip. The hybrid device is 2mmx1.5mmx0.6mm. It also uses a single actuation mechanism, which was driven with a supply of under 30V for the whole tuning range. The tuning was also entirely done away from the main lasing mode in one direction. This means that the system has the potential of twice the tuning range if the actuation mechanism allowed for movement in the opposite direction, which should be considered an induced limitation by the MEMS design.

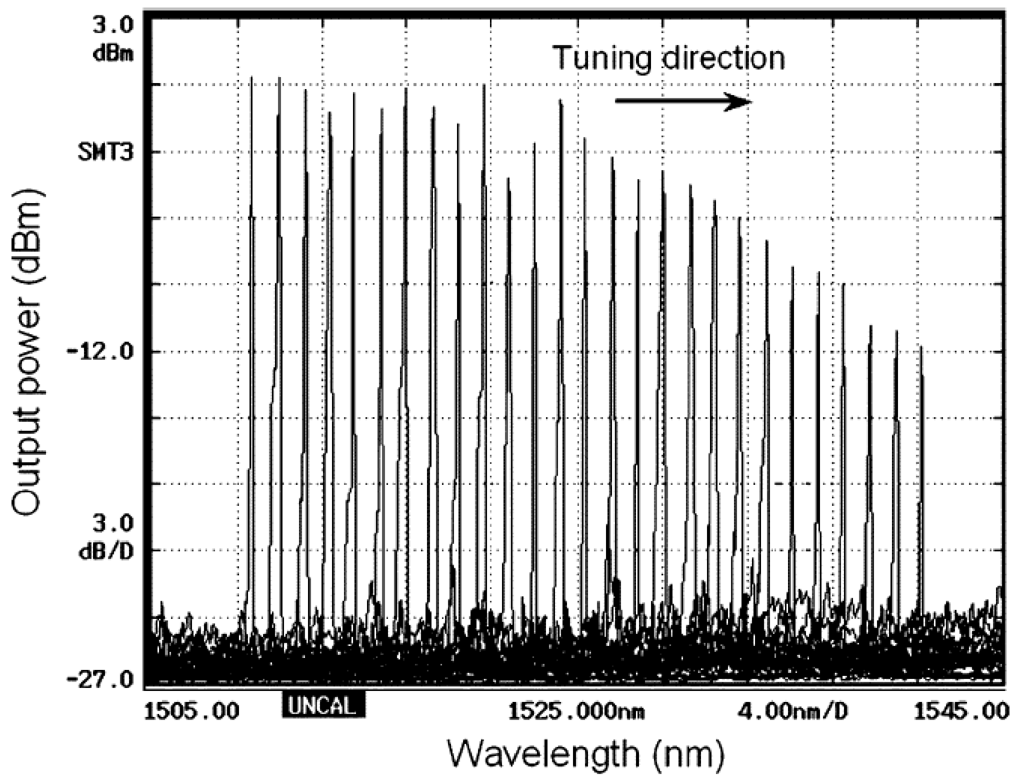

Figure 1.16: Tuning Profile of System Shown in Figure 1.15 [24]

Littman Designs

The Littman geometry by default requires an extra component when compared to the Littrow configuration. However, since the element that needs actuation is the mirror and not the grating the system might be easier to fabricate and faster to tune.

The system [25] shown in figure 1.17 was designed by the group at Imperial. It is a standard Littman configuration, where a diffraction grating is stationary and a mirror is being rotated about a fixed pivot to tune the laser. As has become standard DRIE of BSOI was used to fabricate the mirror and attached actuator as well as the grating. The other components were kept off chip as they did with their Littrow design. 65Nm of tuning was reported with a SMSR greater than 22dB albeit they don't seem to be continuous as shown in figure 1.18.

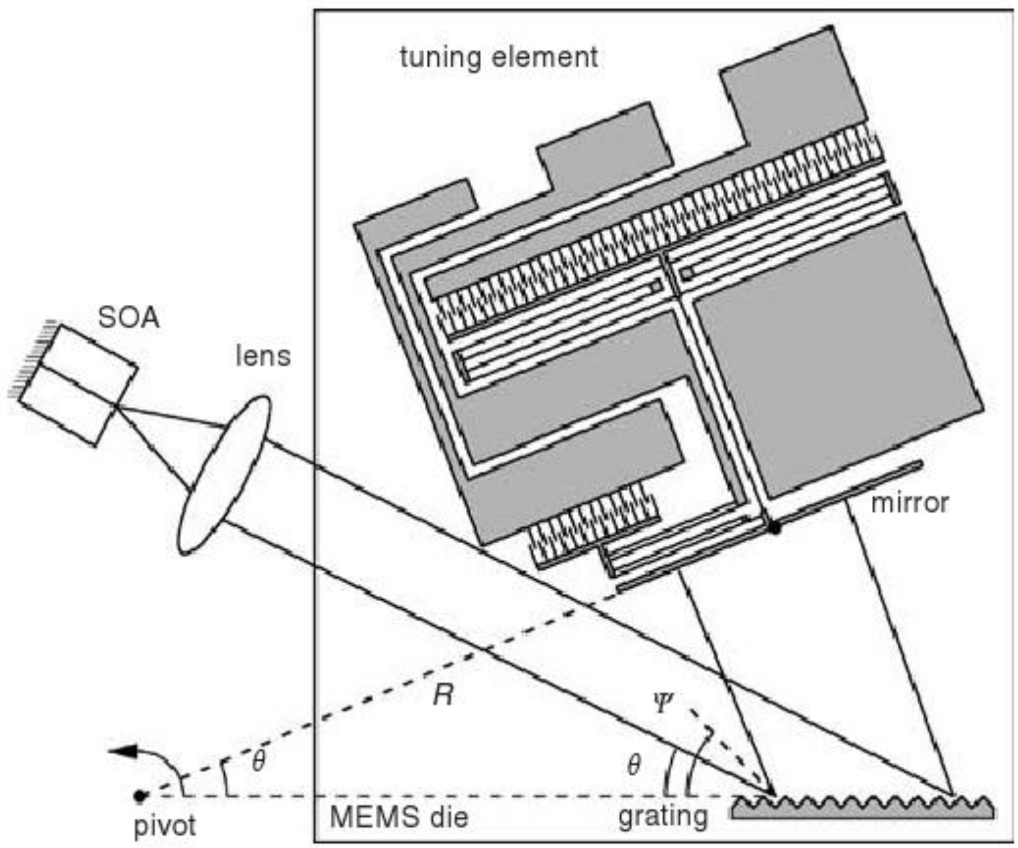

Figure 1.17: Littman ECSL Using Virtual Pivot Point (ICL) [25]

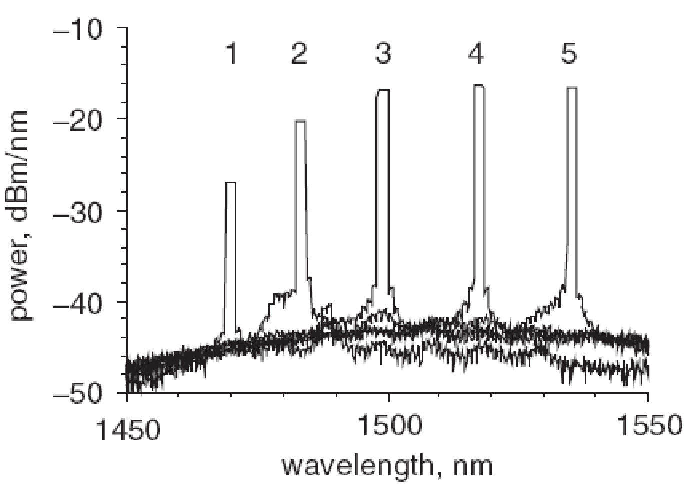

Figure 1.18: Tuning Profile of System Shown in Figure 1.17 (ICL) [25]

An improvement over their Littman design is the actuation mechanism. Again they used two combdrives to render a rotary movement, but this time it was about a virtual pivot point. This design protects the device from extending to a faraway pivot point and enables the realization of devices that might have had unreachable optimal pivot points. The MEMS portion of the device was 5mmx5mm, while the light traveled 13mm in the external cavity.

By far the most polished published MEMS based ECSL design is that of the group at Iolon Inc., California. Their commercial Apollo™ laser [26] is a Littman configuration with a similar idea to that of the Imperial group of having a virtual pivot for the rotary actuation. A rotary combdrive actuator is fabricated using DRIE of BSOI. Their 5mmx5mm hybrid system sweeps through 40nm without mode hopping at a SMSR greater than 55dB as shown in figures 1.19 and 1.20. This design incorporates the ability to rotate the mirror in both directions with a high supply voltage of -140 to 140V. Apollo can also switch from one lasing mode to any other in less than 15ms.

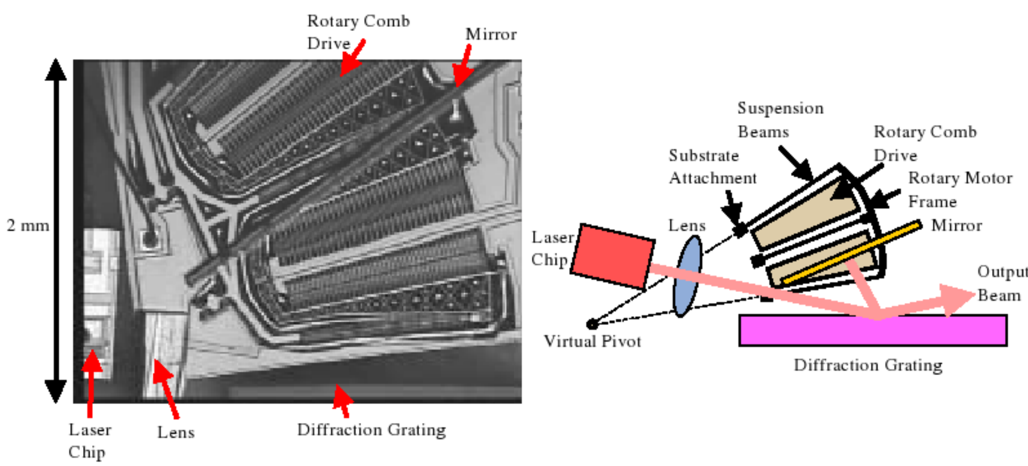

Figure 1.19: Littman ECSL using Rotary Combdrives (Iolon) [26]

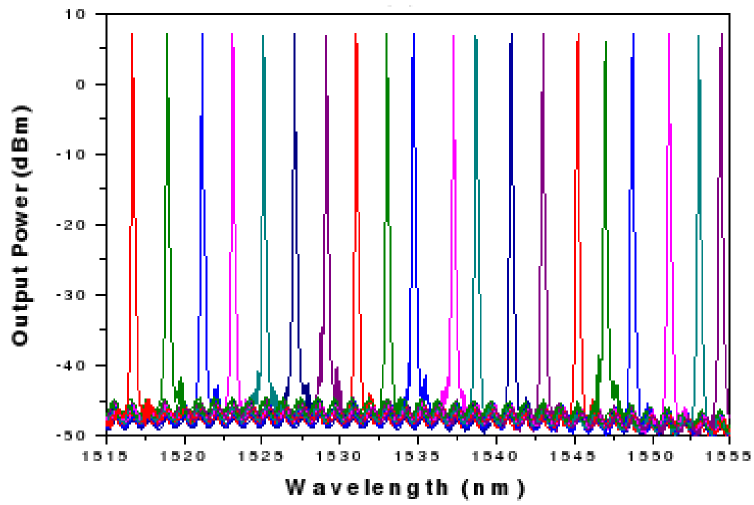

Figure 1.20: Tuning Profile of System Shown in Figure 1.19 (Iolon) [26]

Summary Table

Table 1.1: Summary of some MOEMS attempts to fabricate an ECSL

Group	**Geometry**	**Tuning Range**	**SMSR**	**Tuning Distance**	**Speed (switching time)**	**Tuning Voltage**	**Device Dimensions**
Nanyang University	1-D	16nm	>30dB	10-11µm		10 to 16V	2x1.5mm
		13.5nm	>13dB	66-70µm	2.5kHz (1ms)	2.5 to 18V	1.5x1mm
Imperial College	Littrow	20nm	>20dB	14µm		<50V	
Nanyang University		30.5nm	12-26dB			<30V	2x1.5mm
Imperial College	Littman	65nm	>22dB				5x5mm
Iolon Inc.		40nm	>55dB		(15ms)	-140 to 140V	5x5mm

Thesis Overview

This chapter serves as an introduction to the need for a well-designed ECSL device using MOEMS technology. It highlights the applications for such compact and fast tunable laser devices and explains why a MOEMS ECSL should achieve those specifications. Chapter 1 also explains the background behind this work.

The basic principles of ECSL design are presented followed by a literature review of MOEMS ECSL attempts. Those attempts either underperformed in terms of the resulting tuning range of the device or they sacrificed speed and size resulting from geometrical design constraints. The work in this thesis is an attempt to prove that such sacrifices don't necessarily need to be made if simpler device designs were considered.

Chapter 2 focuses on the modeling of external cavity systems. It makes the trade-off between tuning range and side mode suppression of single ECSLs clear. Then it shows how the idea of adding an extra external cavity would practically resolve this trade off but would introduce mode hops. Chapter 3 further elaborates on how this work extends this idea by moving both mirrors to harvest the design's full two dimensional tuning potential, which eliminates the mode hopping. Chapter 3 also describes how such a device design could be realized using MEMS technology without giving up device size or tuning speed. The results of the conducted proof of concept experiments for a large scale setup are displayed and discussed in chapter 4 along with a description of the experimental setup. In chapter 5 the thesis is concluded and further research recommendations are suggested.

Chapter 2

BACKGROUND

2.1 Single External Cavity

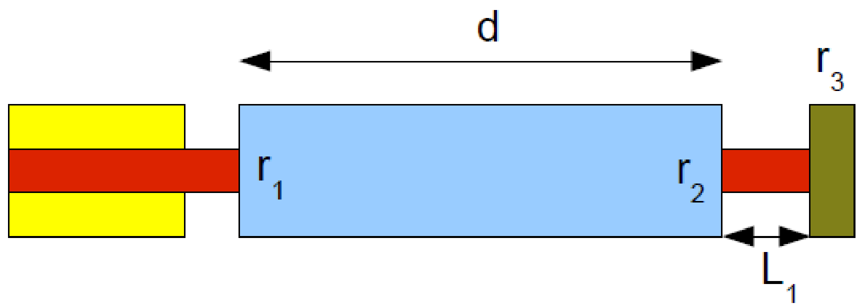

Figure 2.1: 1D ECSL Setup

As shown in section 1.2 the effective reflectivity model reduces the single external cavity system to a regular lasing system with a single internal cavity. The effects of the external cavity on the coherent waves get incorporated into one reflective element described by equation (2.3). The change in the external cavity's length or the external mirror's reflectivity translates in this model to a change in the effective reflectivity. The resulting effective reflectivity is thus a function of the wavelength. Each wavelength in the system will now see a different gain reduction according to the cavity loss profile described by equation (2.2).

$$g_m(\lambda) = g_p - \left(\frac{\lambda_o - \lambda}{G_o}\right)^2 \tag{2.1}$$

$$\alpha_c(\lambda, L_c) = \frac{1}{L_d}\ln\left(\frac{1}{r_1 \mid R_{eff}(\lambda, L_c) \mid}\right) \tag{2.2}$$

$$R_{eff}(\lambda, L_c) = \frac{r_2 + r_3 \exp(-j4\pi\, nL_c/\lambda)}{1 + r_2 r_3 \exp(-j4\pi\, nL_c/\lambda)} \tag{2.3}$$

Equation (2.1) describes a standard parabolic gain profile centered at a specific peak wavelength λ_p. Short cavity III-V semiconductor injection lasers extensively used as the active medium in ECSL design have a gain that can be approximated by the parabolic function [27]. Another factor affecting the power by which the output is emitted is the losses due to absorption in the active region. However since this loss is constant across the range of frequencies we are practically interested in, we'll incorporate this value within the parabolic approximation of the gain profile.

$$g_T(\lambda, L_c) = g_m(\lambda) - \alpha_c(\lambda, L_c) \tag{2.4}$$

The total gain profile as a function of the wavelength and the external cavity length can then be calculated according to equation (2.4) by subtracting the cavity loss profile from the active medium's gain profile. It is now easier to see how moving the external mirror and thus changing the external cavity length would then affect the resulting gain profile so that a different wavelength is at the peak. It is not sufficient, however, to know which wavelength is at the peak of the gain profile. If single mode lasing is required then other modes need to be sufficiently suppressed to ensure that. In this work we used the difference in gain between the main lasing mode and that of the next one in gain magnitude Δg as a measure of side mode suppression.

MATLAB was used to simulate the behavior of the system according to the model described in section 1.2 for different values of the external cavity length. Appendix A includes the code of a more general function that simulates a more complex system as will be discussed later in this chapter. It could also be easily simplified and used to simulate the more generic single external cavity system. Table 2.1 holds a description of the various parameters and their values as assigned to simulate the system.

Table 2.1: Single Cavity ECSL Simulation Parameters and Values

Symbol	**Definition**	**Value**	**Unit**
L_d	active medium length	250	µm
n_d	active medium refractive index	3.4	---
r_1, r_2	reflectivity of original facets	0.32	---
λ_p	wavelength at the peak of the gain curve of the original cavity	1400.33	nm
m	mode number		---
G_o	parabolic gain fitting factor	2 to 7	$nm.cm^{1/2}$
g_p	gain at the peak of the gain curve (incorporates absorption loss)	67.8	cm^{-1}
g_m	active medium gain		---
α_c	cavity loss		cm^{-1}
r_3	reflectivity of external mirror	0-1 (0.32)	---
n_c	refractive index of external cavity	1	---
L_c	external cavity length	0-150	µm
Δg	side mode suppression or difference in gain		cm^{-1}
δL_c	resolution of the change in external cavity length	10	nm
δr_3	resolution of the change in external mirror reflectivity	0.01	---

The effective reflectivity of the external cavity at a specific wavelength is not only a function of the external cavity length as equation (2.3) implies, but also a function of the external mirror's reflectivity. That is why the first simulation involved changing the external mirror reflectivity across the full range from being completely transparent to fully reflective. It also involved sweeping incrementing the value of the external cavity length up to a reasonable value. We chose this arbitrary value to be 150µm. Larger external cavities would contradict our goal of miniaturizing the ECSL device.

The contour plot in figure 2.2 shows the side mode suppression as a function of both external cavity length and external mirror reflectivity. This simulation assumed the original laser had a reflectivity of 0.32 on both sides of the cavity. We can conclude from the output that the best external cavity reflectivity in the case of a single external cavity in terms of side mode suppression is for the external cavity mirror to match the reflectivity of both internal mirrors. This result helped reduce the complexity of further simulations. It eliminated the need to vary the external mirror's reflectivity.

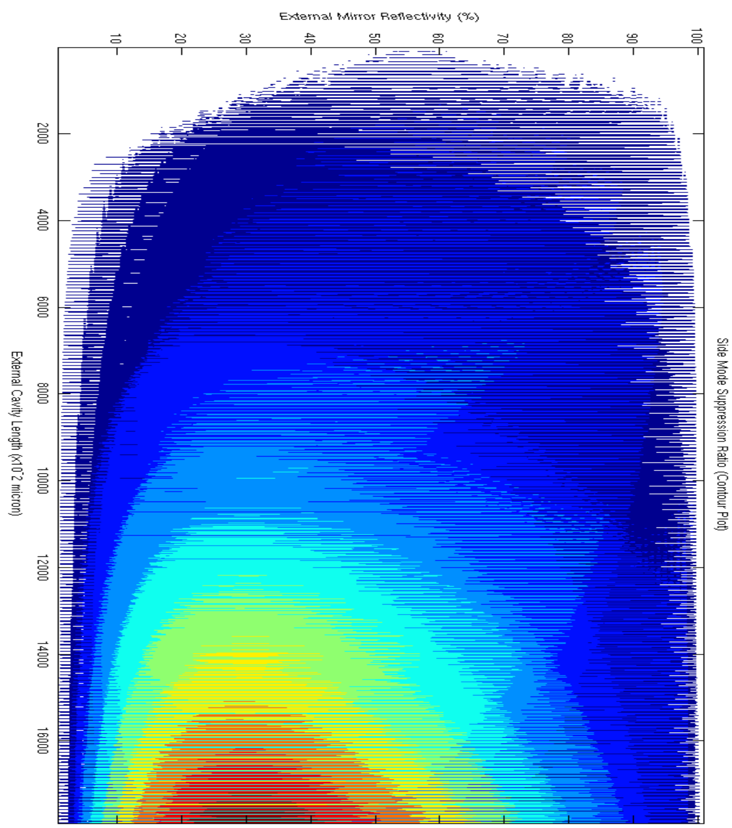

Figure 2.2: Contour Plot of SMSR

Another very important observation is the enhancement of side mode suppression as we put the external mirror further away from the original laser source. This can be understood in light of the increased spacing between the resonating modes that are commonly selected by both the original and the external cavity. This makes it easier to filter out neighboring modes and select the desired lasing mode.

The problem, however, with extending the length of the external cavity is the limitation that imposes on the tunable range of the laser. Fewer modes fall within your tuning distance because of the modes being spaced out and the fact that the distance, over which you can tune between modes before they start repeating, is constant independent of the length of your external cavity. This trade off between side mode suppression and tuning range sums up the limitation of this tuning geometry, which only allows for one degree of freedom; namely the length of the external cavity.

The tuning distance can be found by observing equation (2.3). Considering that the tuning range is small compared to the value of the wavelength we can assume it is constant for this purpose at its nominal value. In equation (2.3) it is obvious that the two rotating exponentials will take on values from negative one to one repeating within a fixed tuning distance. The tuning distance ΔL_t can be described by the following relation:

$$\Delta L_t \sim \frac{\lambda}{2\mathrm{n}} \tag{2.5}$$

2.2 Dual Cavity 1D Tuning

The simple geometry discussed in section 2.1 is well suited for miniaturization, but it suffers from certain limitations. A tuning range cap is imposed, if single mode lasing was desired, by the side mode suppression. To increase the tuning range one needs to increase the external cavity length or design a laser with a wider medium gain profile. Both cases favor competing modes as well, which negatively affects the side mode suppression.

This led researchers to investigate alternative ECSL design geometries that allow for an extra filtering mechanism that would enhance side mode suppression without affecting the laser's tuning range. The most popular geometries designed to achieve that were the Littman/Metcalf [28] and the Littrow (E.g. [23]) grating based ECSL configurations. MEMS based designs followed suit, but as demonstrated in chapter 1 those designs aren't very miniaturization friendly. The presence of a grating and the need to rotate about a pivot point in addition to being forced to have longer external cavities and having to add a lens to overcome the effects of that are all factors that render miniature grating-based ECSL designs complex, slow, bulky and non-monolithic.

A less popular design addressing the limitations of the basic ECSL design with a single tuning element is the dual cavity design by Zhu and Cassidy [29]. Figure 2.3 shows an illustration of the dual cavity setup. A second fixed mirror is placed on the other side of the original cavity forming a second external cavity between the laser and the fiber. This mirror needs to have low reflectivity to allow most of the light to be collected as the system's output.

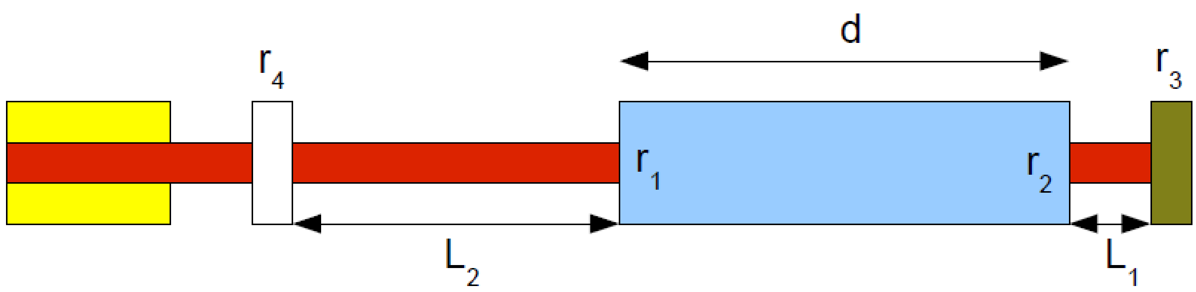

Figure 2.3: Dual External Cavity Semiconductor Laser Setup

The Zhu/Cassidy configuration was very successful in most aspects. One reflective movable element was used as usual for tuning and was placed fairly close to the original cavity (Lc_1~10μm) for a wide tuning range. The other, mostly transparent, mirror was placed further from the cavity (Lc_2~150μm) to ensure good side mode suppression. They achieved a wide tuning range of 72nm with a SMSR greater than 20dB [8], [29]. These results came at the cost of continuous tuning. As opposed to the grating-based configurations that allow for continuous tuning through all possible modes the dual cavity configuration with one moving mirror skips some modes and enhances others.

From a fabrication perspective the dual cavity configuration reduces complexity and size constraints by eliminating rotary movements and reducing the external cavity size. It also does not require a grating and it reduces the linear motion required to go through all possible modes back down to the tuning length discussed earlier in section 2.1. On the other hand it showed a deficiency in continuous tuning.

A dual cavity laser can be modeled as well using the effective reflectivity principle. In this configuration we'll have two effective reflectivities to represent the two external cavities and their elements. Similar to equation (2.3) equations (2.6) and (2.7) describe the effective reflectivities of the first and second external cavities respectively. Equation (2.8) shows how we gained a new variable to influence the cavity loss at a particular wavelengthλ.

$$R_{eff1}(\lambda, L_{c1}) = \frac{r_2 + r_3 \exp(-j4\pi\, nL_{c1}/\lambda)}{1 + r_2 r_3 \exp(-j4\pi\, nL_{c1}/\lambda)} \tag{2.6}$$

$$R_{eff2}(\lambda, L_{c2}) = \frac{r_1 + r_4 \exp(-j4\pi\, nL_{c2}/\lambda)}{1 + r_1 r_4 \exp(-j4\pi\, nL_{c2}/\lambda)} \tag{2.7}$$

$$\alpha_c(\lambda, L_{c1}, L_{c2}) = \frac{1}{L_d} \ln\left(\frac{1}{| R_{eff1}(\lambda, L_{c1}) || R_{eff2}(\lambda, L_{c2}) |}\right) \tag{2.8}$$

Our simulation for a dual cavity configuration with one movable highly reflective mirror placed close to the original cavity and a fixed highly transparent mirror placed further away on the other side of the cavity matched the experimental results achieved by Zhu/Cassidy setup. The parameters and their values in the simulation are presented in table 2. Appendix A lists the MATLAB script that was used for the simulation in section 3.1.3. However, it can be easily altered by fixing the second external cavity's length at the value in table 2.2. For comparison purposes a single cavity system with the same parameters following the model explained in 2.1 was simulated.

Figure 2.4 shows how the Zhu/Cassidy setup, compared to the single cavity configuration, drastically improved side mode suppression values while maintaining the same tuning range possible by the latter. Even though theoretically the graph result for the single cavity simulation shows a wide tuning range with the ability to tune to all possible modes in the range, those modes would never lase in single-mode because of the very poor side mode suppression. Competing modes are not suppressed enough for single-mode lasing. The dual cavity configuration makes this range possible because the limited available modes can all be tuned to at high side mode suppression values.

The presence of the second cavity to enhance side mode suppression relaxes the constraints placed on the system. It does not eliminate the tradeoff between tuning range and side mode suppression, but it pushes this barrier back by a significant factor. Figure 2.5 shows a simulated system with an active medium that has a wider gain profile.

A much wider tuning range resulted with acceptable side mode suppression. This wouldn't have been possible with the simpler configuration.

Table 2.2: 1D Dual Cavity ECSL Simulation Parameters and Values

Symbol	**Definition**	**Value**	**Unit**
L_d	active medium length	250	µm
n_d	active medium refractive index	3.4	
r_1, r_2	reflectivity of original facets	0.32	
λ_p	wavelength at the peak of the gain curve of the original cavity	1400.33	nm
m	mode number		
G_o	parabolic gain fitting factor	2 to 7	nm.cm$^{1/2}$
g_p	gain at the peak of the gain curve (incorporates absorption loss)	67.8	cm^{-1}
g_m	active medium gain		
α_c	cavity loss		cm^{-1}
r_3	reflectivity of highly reflective external mirror	0.32	
r_4	reflectivity of highly transparent external mirror	0.04	
n_c	refractive index of external cavity	1	
L_{c1}	first external cavity length	~10	µm
L_{c2}	second external cavity length	150	µm
SMS	side mode suppression		cm^{-1}
N/A	resolution of the change in external cavity length	10	nm

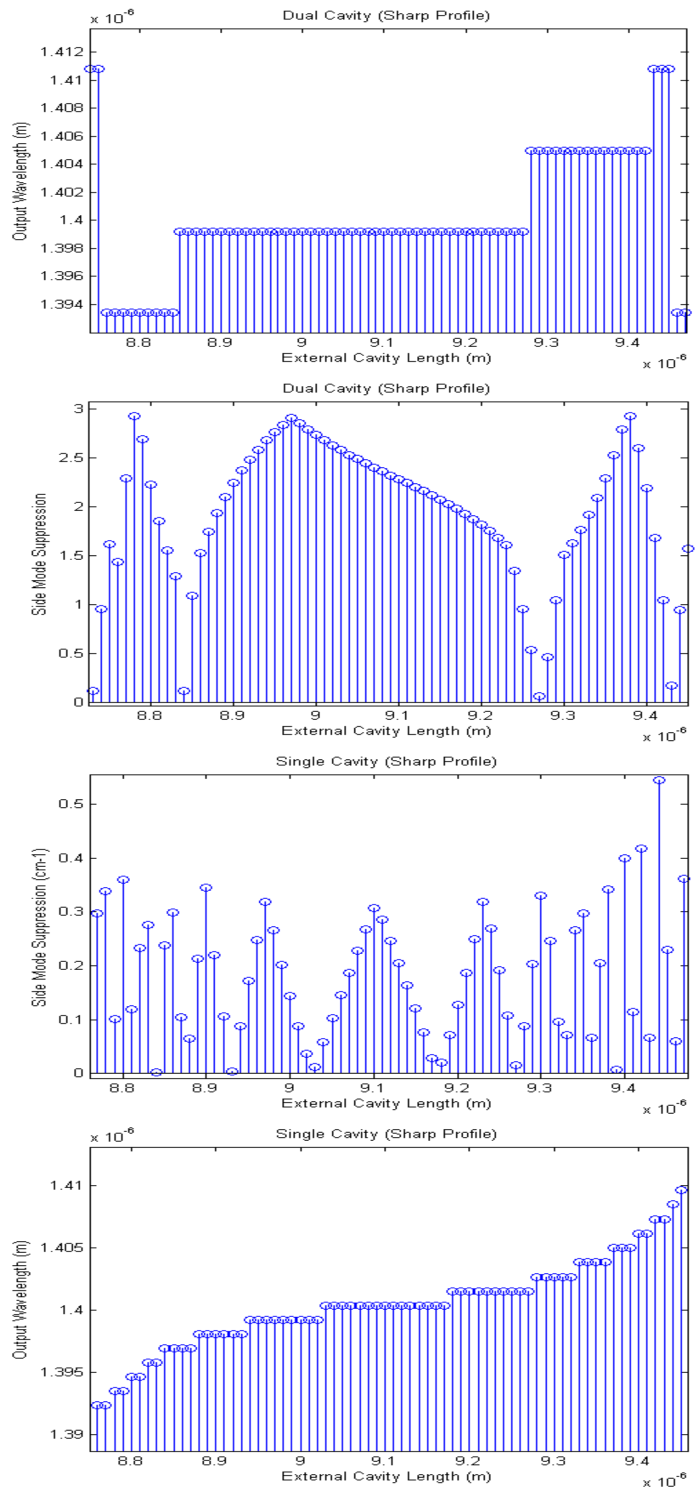

Figure 2.4:Improved SMS with a Dual Cavity Setup

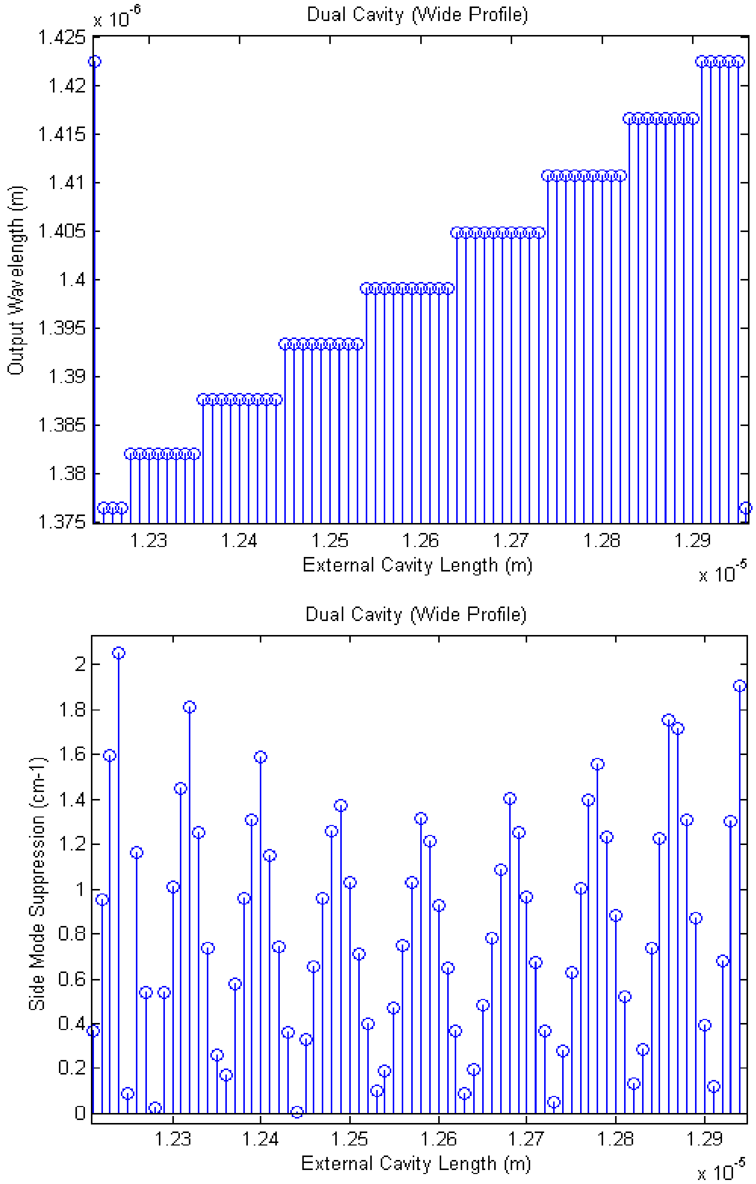

Figure 2.5: Wide Discrete Tuning Range with Dual Cavity Setup

Chapter 3

SYSTEM DESIGN

3.1 Dual Cavity 2D Tuning

As explained in section 2.2 the Zhu/Cassidy setup is superior to the single cavity setup and is still simpler and more useful to fabricate on a MEMS die than the grating based designs critiqued in chapter 1. The simulations in this section will show how the dual cavity configuration was not used to its full potential. This will explain why mode-hopping was observed and how it could be overcome.

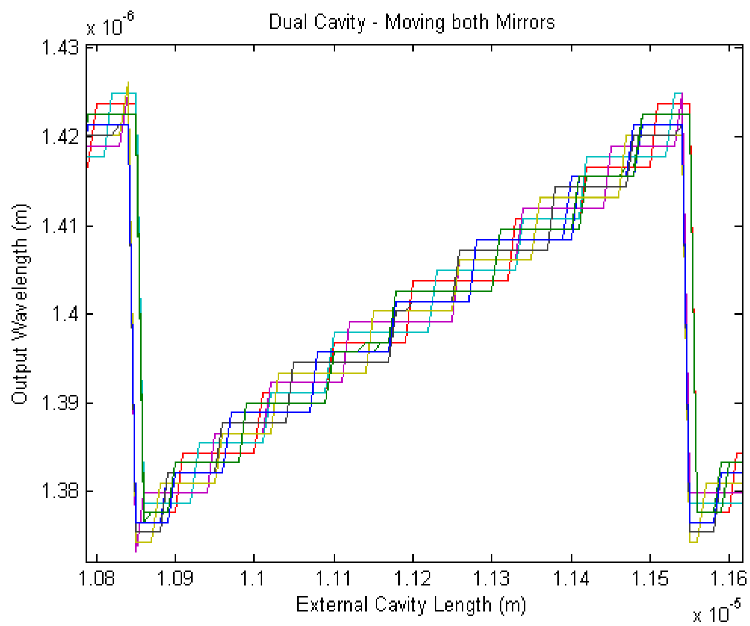

Figure 3.1: Overlay of Simulation Output of a Dual Cavity Setup

Figure 3.1 shows the graph result of a dual cavity simulation with one fixed mirror and one movable mirror same as the simulation in figure 3.1. It displays an overlay of simulation with the same setup with a different fixed second external cavity length. Every color represents a different L_{c2}. Each simulation achieved the same results of covering a good tuning range while hopping several modes in the range and enhancing others. The enhanced modes for every second external cavity length were different and the combination of all results would yield a continuously tunable setup.

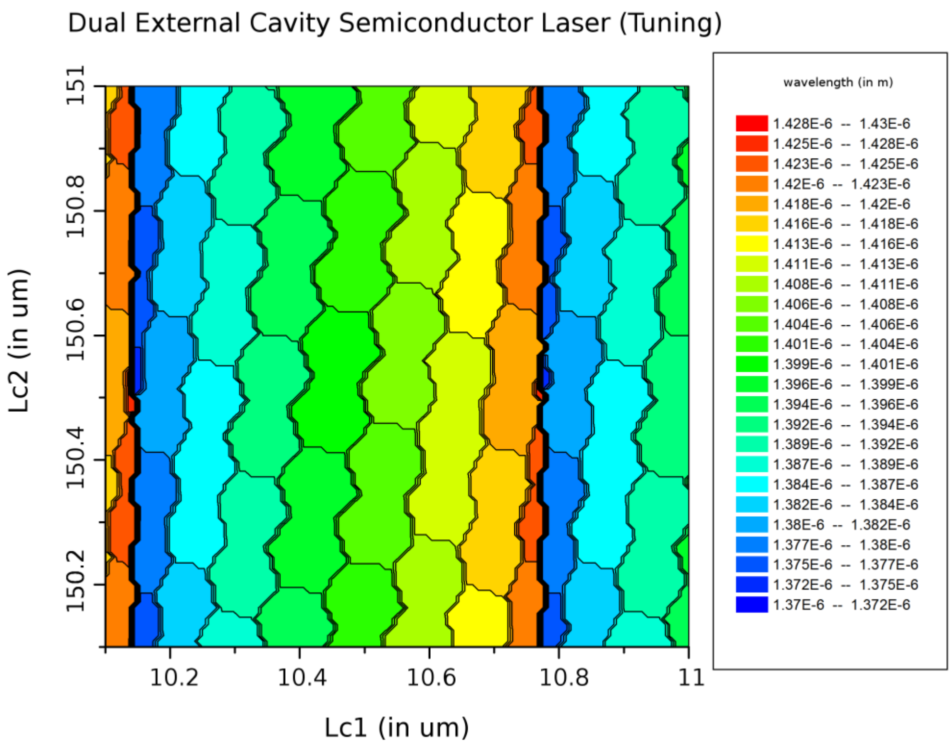

Figure 3.2: Contour Plot Mapping the Main Mode of a Dual Cavity Simulation

A more visual representation of this idea can be seen in figures 3.2 and 3.3, which respectively display the tuning range and side mode suppression results of a dual external cavity semiconductor laser with two movable mirrors. The MATLAB code in Appendix A was used to produce this simulation. It represents a MATLAB function that takes as input the ranges of L_{c1} and L_{c2}, sweeps through those values in 10 nm increments and produces two contour plots that represent the dominant wavelength of the system and the value of the side mode suppression at every value of L_{c1} and L_{c2} in the given range. The function also stores the results in an ASCII file for further analysis. This analysis will be further described later in this section.

This simulation clearly displays the power of having control over both cavity lengths. For every possible lasing mode in the tuning range there exist two external cavity lengths that would amplify the suppression of its competing modes. It is very visible from figure 3.3 that it is not possible to go through the side mode suppression peaks without changing the length of the second cavity. Each hexagonally shaped region representing the dominance of a particular lasing mode in figure 3.2 has an equivalent cone shaped side mode suppression profile with a hexagonal base in figure 3.3. The cone's peak is at the center of the hexagon.

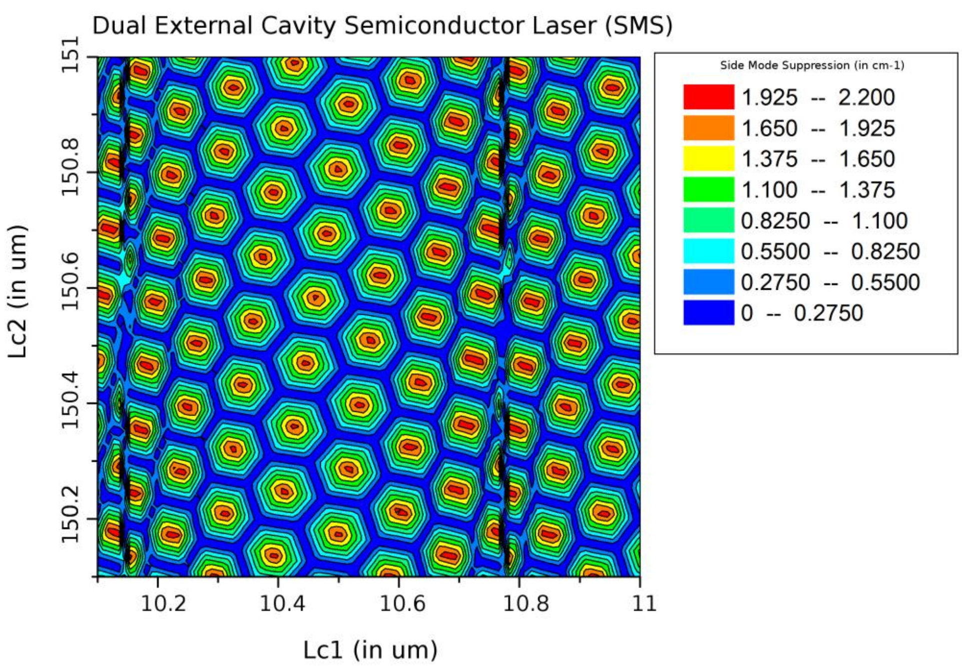

Figure 3.3: Contour Plot Mapping the SMS of a Dual Cavity Simulation

From there we suggest that the non-continuous tuning limitation of the dual external cavity geometry can be eliminated by the movement of the second mirror. The Zhu/Cassidy configuration can be represented by a horizontal line cutting through both contour plots, which would explain the mode-hopping observed by their experiment.

We conducted a more general simulation and analysis to highlight the optimal regions to be used in an experimental setup. The MATLAB function in Appendix A was used to generate ASCII data files containing the dominant wavelength output of the system and the side mode suppression value at every generated L_{c1} and L_{c2} value in a 2μmx5μm range. The external cavity lengths were generated at a resolution of 10 nm as the previous simulations. This function was called in a loop to cover a full simulation range of $L_{c1} \times L_{c2} = 50\mu m \times 250\mu m$. However, each 2μmx5μm output was stored in a separate data file for analysis purposes. The analysis results are displayed in figures 3.4-7. Table 3.1 defines the parameters presented in this analysis.

Table 3.1: Parameter Definition of Extended Dual Cavity ECSL Simulation

Parameter	**Definition**	**Unit**
2-D Analysis Resolution	The smallest simulated unit that represents one value in the analysis graphs. $L_{c1} \times L_{c2} = 2\mu m \times 5\mu m$	$(\mu m)^2$
Tuning Range	The difference between the maximum and minimum wavelength output values produced by the system in every simulated unit.	nm
Peak Side Mode Suppression	The maximum side mode suppression value in the simulated unit.	cm^{-1}
Average Side Mode Suppression	The average of all side mode suppression values in the 2-D simulated unit.	cm^{-1}

There is no surprise that the closer the tuning mirror is from the original cavity, the wider the tuning range. At the same time placing the mirrors away from the original cavity improves the side mode suppression. Figures 3.4, 5 and 6 confirm these rules of thumb. Figure 3.4 also shows that the second mirror has little effect on tuning and that this effect vanishes as the second external cavity length is increased beyond around twice the value of the first external cavity length.

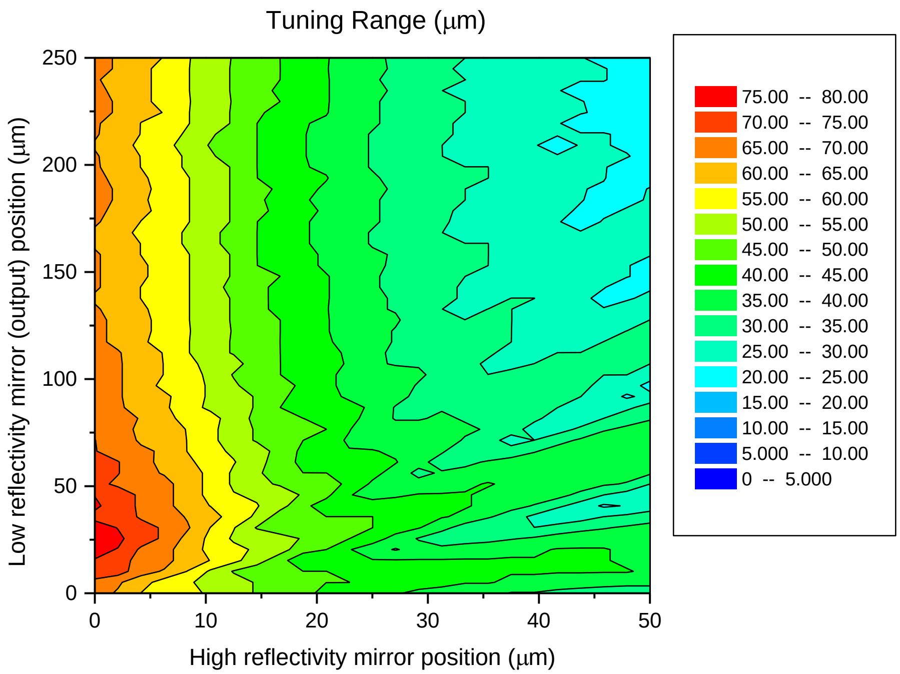

Figure 3.4: Dual Cavity ECSL Analysis – Tuning Range Contour Plot

It is also important to note that figures 3.5 and 6 show that at specific second external cavity lengths decent side mode suppression values are possible at very short first external cavity lengths. This translates to wide tuning ranges at around 150, 170 and 240μm.

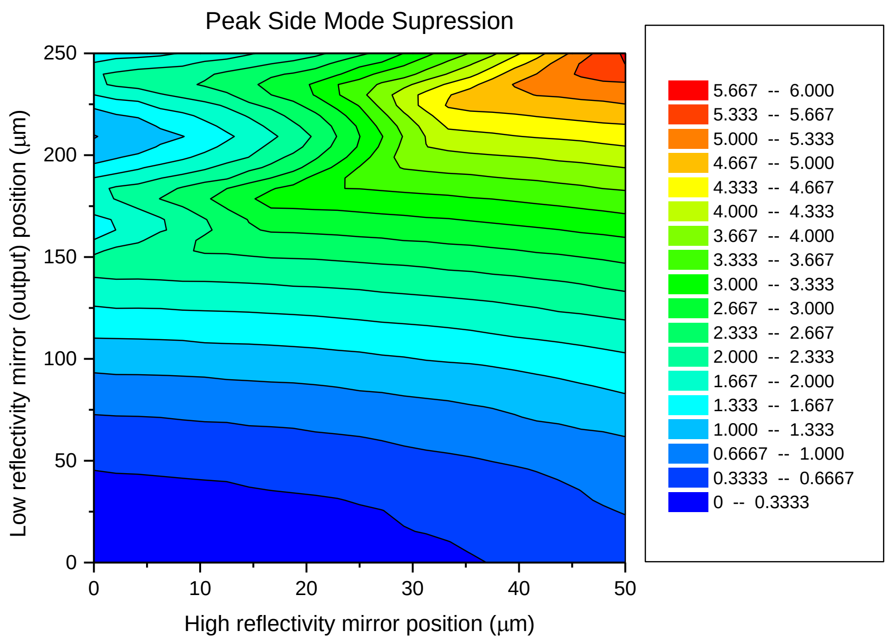

Figure 3.5: Dual Cavity ECSL Analysis – Peak SMS Contour Plot

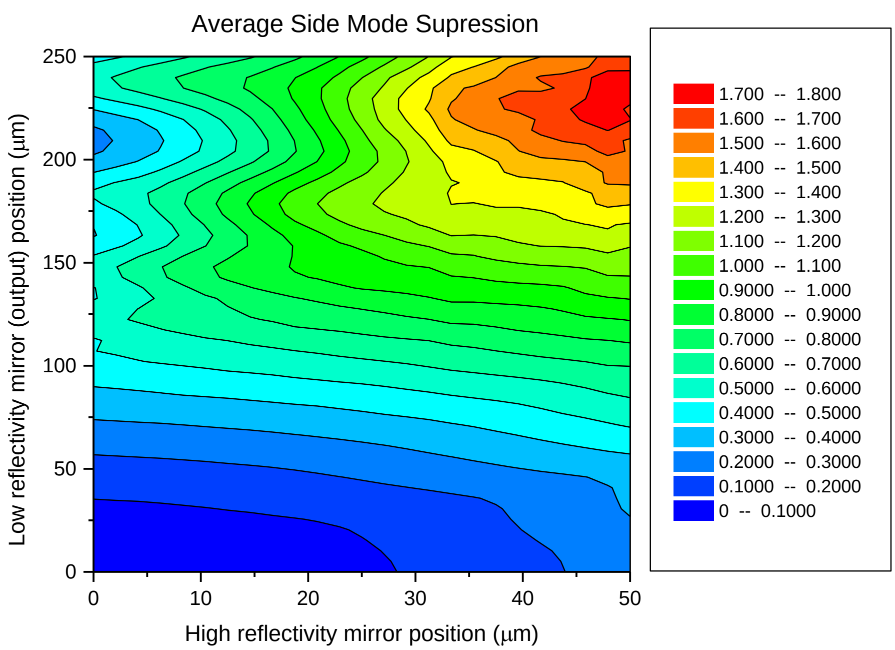

Figure 3.6: Dual Cavity ECSL Analysis – Average SMS Contour Plot

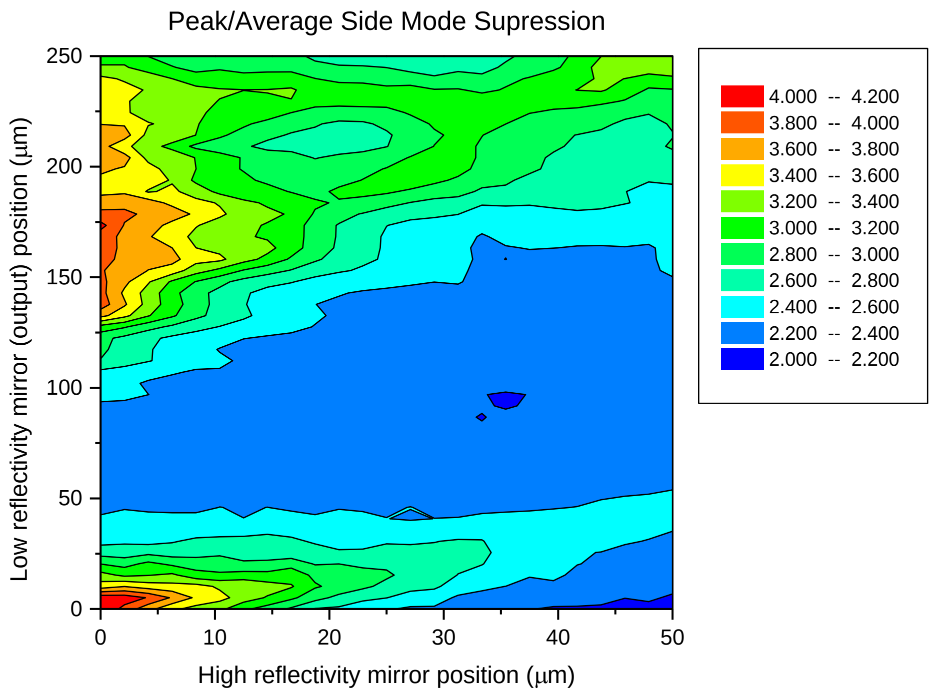

Figure 3.7: Dual Cavity ECSL Analysis – SMS Peak to Average Ratio Contour Plot

3.2 Device Design Improvements

This section is not meant as a comprehensive device design of a MEMS ECSL leveraging the 2D-dual cavity tuning principle introduced in this work. It is rather just a collection of preliminary simplified design calculations that demonstrate the advantages of using this new principle at the micro scale.

To achieve a reasonable tuning range with acceptable side mode suppression a 2 dimensional setup was needed. This drove the device dimensions to the millimetre range for numerous reasons. The size of the grating element is not the main problem but rather the distance to the pivot point at which the element needs to be placed to achieve continuous tuning in addition to the relatively large micro actuators used to move the elements to lock into the desired mode.

In the case of the dual external cavity setup we are proposing there are a number of constraints that affect device size. We will discuss those to demonstrate the size reduction made possible by our technique.

3.2.1 Length of External Cavities

The nominal positions of the mirrors are dictated by the optimization of maximizing the tuning range and the side mode suppression. From examining figures 3.4-7 we can deduce that the highly reflective mirror needs to be very close to the original cavity to allow a wide tuning range. This mirror will be located within 10µm of the facet. The second external cavity needs to be around 150µm long for acceptable side mode suppression. This makes the length of our device at least 160µm longer than the original laser.

3.2.2 Tuning Distance/Actuation Technique

Zhu cited [8] a tuning distance beyond which the laser output will cycle back again through the same set of modes. This is also very evident by examining the effective reflectivity model. The exponentials of equation (2.3) have the period $\lambda/_{2n}$. As a result of that the simulations show the same periodicity in tuning for both external cavity lengths. Figure 3.2 shows that in the specific case when λ is around 1.5µm the mirrors need only be swept over 0.7µm.

The significance of the tuning distance is that it has a profound effect on the technique used to perform the mirror actuation. The other factors are the size of the mirror and the profile of the motion. Moving a big structure over a relatively long distance around a distant pivot point can be a cumbersome task. For those reasons comb drives have been the actuators of choice in most MEMS ECSL attempts [21], [22], [24-26].

In our case the small tuning distance required can be achieved by a much simpler actuation method based on deflection. The benefit is more than just the simplicity of the MEMS design but rather also the speed by which this actuation can be done.

3.2.3 Preliminary Calculations

To put the claims made in the two previous sections to the test we will attempt to envision a basic preliminary design of a MEMS based ECSL.

This design consists of a cavity etched out to host an external diode laser. This cavity is surrounded by 2 vertical mirrors that have been etched out and released from both faces and from below but are still attached at their sides. The two mirrors will be electrostatically actuated by controlling a voltage charge at the other side of the mirror. The mirrors will deflect away from and towards the laser to cause the change of length of the external cavities.

Table 3.2 reflects some assumptions for a basic mirror actuation concept so that we can estimate through our preliminary calculations the order of magnitude of the voltage required to be applied to induce the maximum deflection of the system as well as the frequency of resonance of the structure to have a good indication of how fast the tuning can be achieved. The assumptions made are based on the results from the simulations, the experiments done by us and others, and best estimates.

After being released from below the mirror shown above in figure 3.8 can be modeled as a beam that is hinged from both ends with a distributed electrostatic force applied along its length. The equations and calculations needed to find the voltage required for the desired deflection and the resonant frequency of the mirror can be found in appendix B. Attached in appendix B is also the python script used to do the final calculations based on the assumptions made in table 3.2.

Table 3.2: Assumptions of basic concept for preliminary calculations

Symbol	**Definition**	**Value**	**Unit**
l	mirror length	150	μm
H	mirror height	60	μm
T	mirror thickness	2	μm
d	air gap	5	μm
y_{max}	maximum deflection needed to sweep across all modes	1	μm

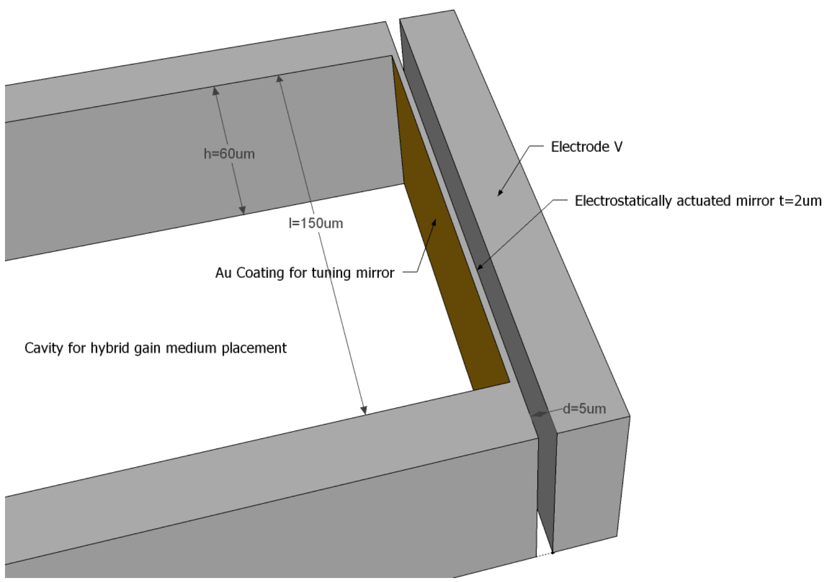

Figure 3.8: 3D Illustration of basic SOI Concept for Mirror Actuation

We estimate that this setup made possible by the dual external cavity concept would reduce the form factor to roughly 300μm x 200μm x 200μm. The voltage required to tune through all the modes is < 40V and the resonant frequency of the mirror is in the 10’s of MHz order of magnitude.

Chapter 4

EXPERIMENTAL MEASUREMENTS & FINDINGS

4.1 Experimental Setup

A multiple quantum well broad gain profile semiconductor laser, lasing at 1.4μm in multimode, was aligned between a spherical mirror and the tip of an optical fibre cable. The laser had a short cavity of 250μm. A short external cavity was created between the back facet of the laser and the copper coated spherical mirror. All elements were attached to 3-axis stages for alignment purposes. The length of the external cavity was controlled by changing the voltage value applied to a piezoelectric actuator attached to the mirror. That was achieved by a voltage driver, which was amplifying the output signal of a digital to analog converter card on a PC. The fibre cable was connected to an input terminal on an Anritsu optical spectrum analyzer (OSA) to display the resulting laser spectrum. The OSA was attached to the same PC through a general purpose interface bus (GPIB) instrument interfacing card and connector.

A LabVIEW virtual instrument (VI) was used for both control and data acquisition. The VI shown in figure 4.2 is at the top of the program's hierarchy. The routine automates the experiment by generating a voltage value for each piezo-actuator's controller, which in turn defines the mirror's position. It also triggers the OSA and acquires the laser's output spectrum as measured by the instrument.

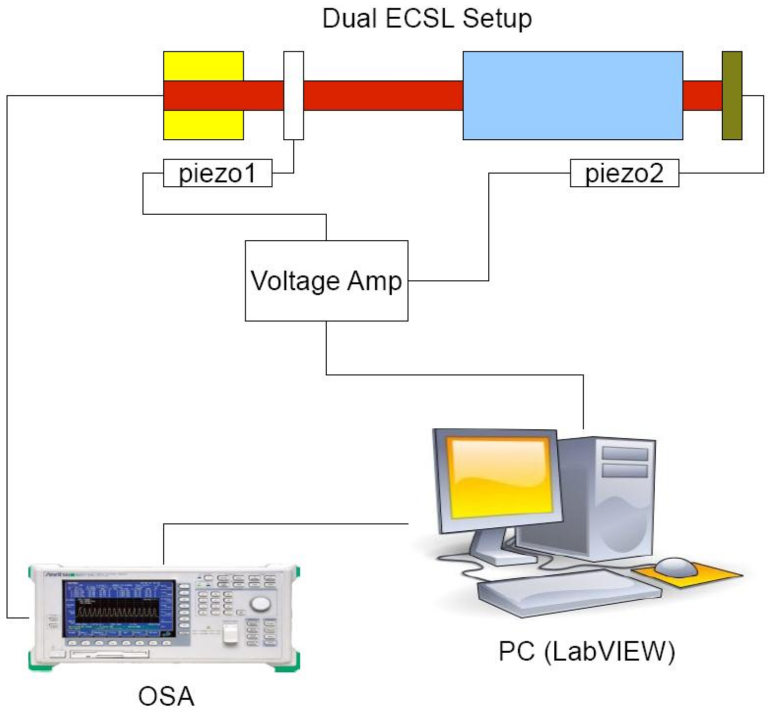

Figure 4.1: Experimental Setup

The block diagram depicts how the code automates the measurement process to sweep through a range of external cavity lengths between both mirrors and the original cavity. Two nested loops are used so that every increment of the short cavity's length is appended by a full sweep of the second external cavity.

For every move of the second external cavity the output of the OSA is saved with a stamp indicating the length of both cavities when the data was captured. A short delay is positioned between the move and the data capture to allow the system to settle.

Alternatively the experiment was set up to allow for manual control as well. In that case a knob on each voltage supply connected to their respective piezo actuators controlled the position of the mirrors.

To rule out a number of factors that are not of great interest for the purpose of this proof of concept we gradually altered the setup to compare the different configuration concepts. All other factors were kept as consistent as possible. A current source driving the original semiconductor laser was maintained at the same level for all experiments.

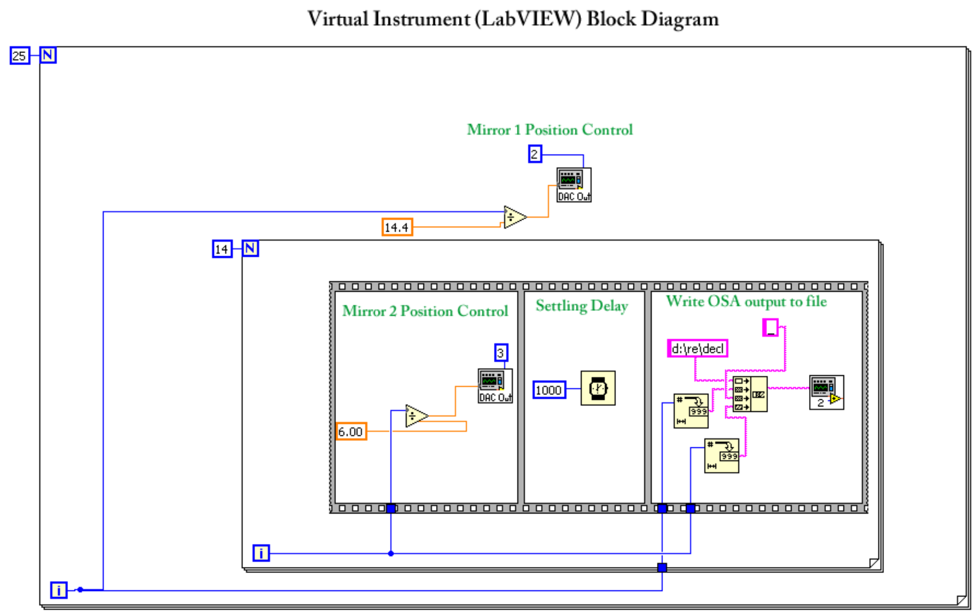

Figure 4.2: Automated Experiment Code Block Diagram

In all configurations the same gold plated spherical mirror was used and the alignment of which was not tampered with. The secondary mirror was a thin piece of glass, which was used only in the dual cavity configuration between the laser and the fibre. The fibre alignment and position with respect to the laser was unchanged.

4.2 Measurements & Findings

4.2.1 Single Cavity Measurements

In the single cavity configuration 3 external cavity lengths were attempted to study the effect of the proximity of the mirror to the laser on the mode selection and the side mode suppression.

Figure 4.3 shows three different output readings each corresponding to a different mirror position within the tuning distance of the mirror. In this case the mirror was approximately 15µm away from the active medium. At this short distance you can get the widest tuning range possible by the given system. However, as is highlighted in the figure, the side mode suppression is minimal preventing single mode lasing.

Figure 4.4 shows the effect of moving the mirror away from the active medium. At the 70µm mark for this configuration a good balance between single mode operation and tuning range is achieved. The optimal operating point for the elements used in this setup in a single cavity configuration is an external cavity that is shorter than 70µm.

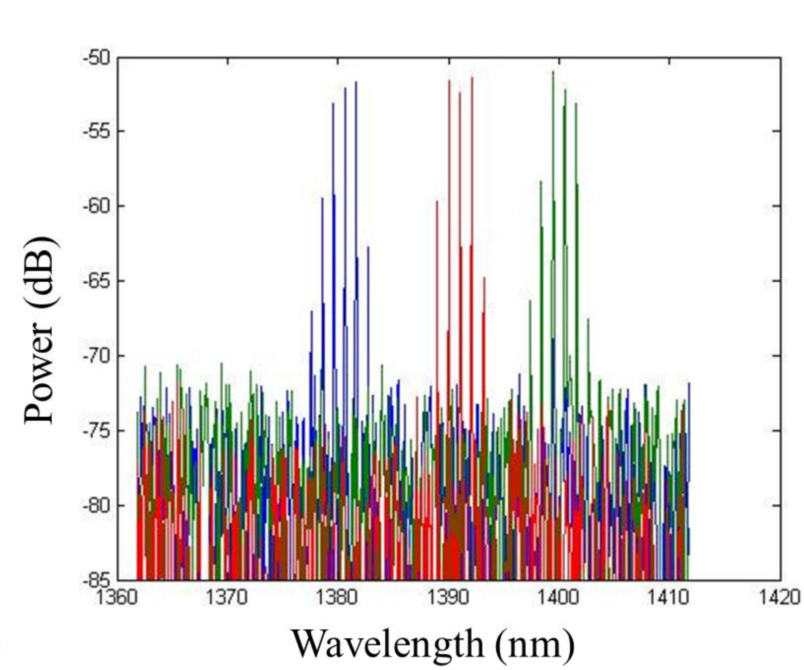

Figure 4.3: Short Single External Cavity Tuning Results

By moving the mirror even further away from the active medium the side mode suppression is enhanced and the allowable tuning range within the same fixed tuning distance shrinks. This can be seen in figure 4.5.

Average External Cavity Length	**Tuning Range**	**Side Mode Suppression**
~15 µm	~20 nm	(multimode)
~70 µm	~8 nm	>20 dB
~150 µm	~5 nm	>30 dB

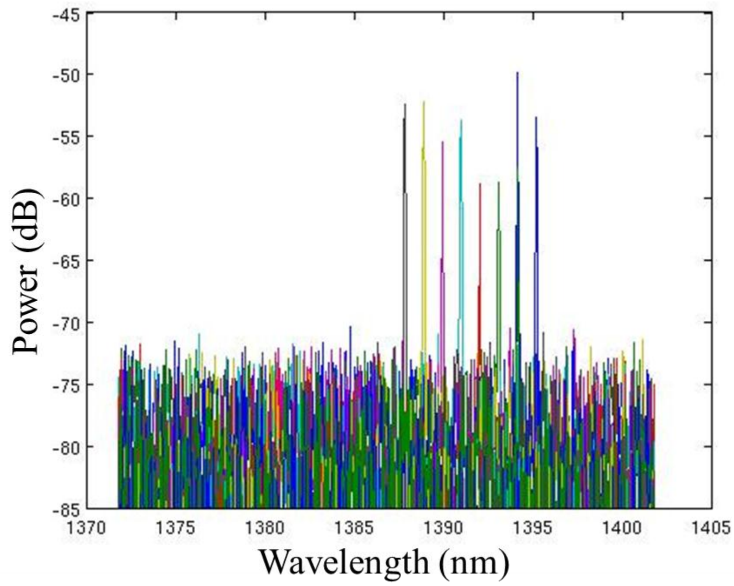

Figure 4.4: 70μm Single External Cavity Tuning Results

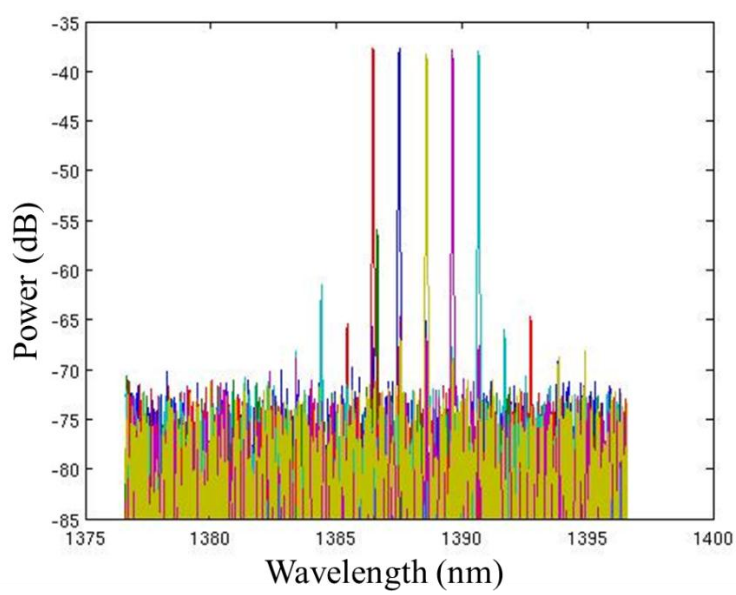

Figure 4.5: 150μm Single External Cavity Tuning Results

4.2.2 Dual Cavity Measurements

A couple of dual cavity scenarios were attempted to showcase the value of the concept proposed in this work. The first scenario is a replica of the Zhu/Cassidy configuration. A highly transparent sheet was placed between the laser's facet and the fibre. The output of the system still comes from that side through the new element. The low reflectivity of this element is sufficient to aid with the side mode suppression. In this configuration the element is kept static and tuning is achieved by moving the highly reflective mirror placed on the other side of the active medium to for a very short external cavity of 10 to 15µm.

Figure 4.6 below shows the output achieved from this configuration. By comparing that with figure 4.3 shown earlier we can see the benefit of adding the secondary mirror. Much better side mode suppression is allowed while retaining the tuning range made possible by the short external cavity. The drawback as discussed by Zhu [8] and in accordance with the simulation results presented earlier in this work is the mode hopping effect shown in figure 4.6. Only the modes shown in the figure were allowed to lase.

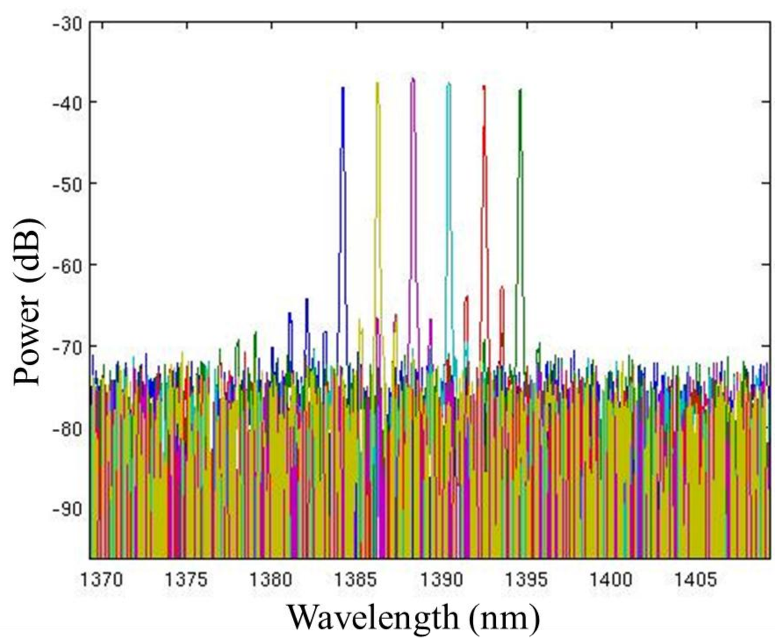

Figure 4.6: Dual Cavity 1D Tuning Results (Zhu/Cassidy)

As argued earlier in this work and confirmed by the presented simulation results the reason why the Zhu/Cassidy configuration exhibits mode hopping is the fixed position of the secondary reflective element. The fixed second external cavity length only allows specific modes to resonate while suppressing others. The first external cavity can only select, in this case, the modes allowed by the second external cavity.

To overcome the mode hopping we proposed controlling the position of the secondary tuning element as well. A piezo actuator was attached to the transparent sheet to permit control of the second external cavity. The output shown in figure 4.7 confirms the simulation results presented earlier in this work suggesting that continuous mode tuning is possible using the Zhu/Cassidy dual cavity configuration. Only modes with a side mode suppression > 20dB are shown in figure 4.7. One mode in the ~18nm range was skipped because of that requirement.

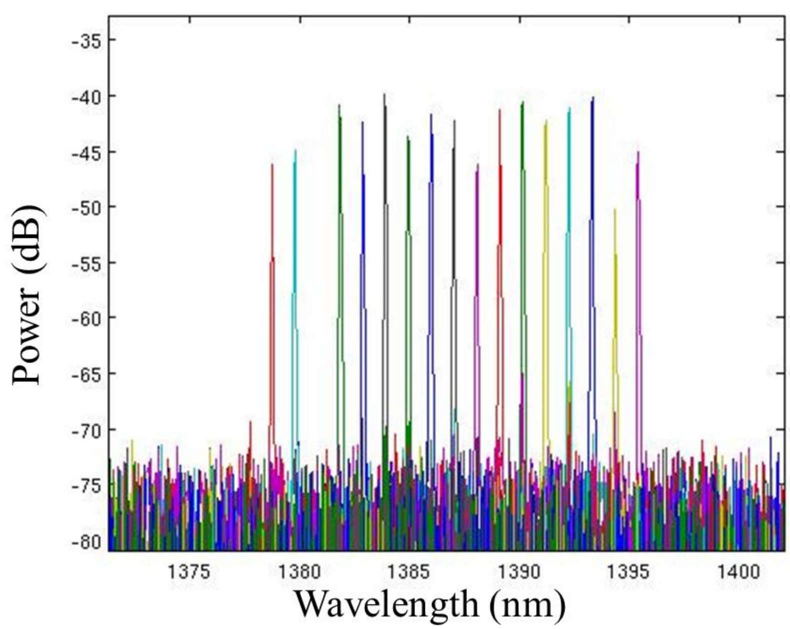

Figure 4.7: Dual Cavity Tuning Results

4.3 Discussion

4.3.1 Automated Measurements

The automated measurements described in the previous section aimed at mapping the output of the laser for every position of the mirrors. This would have allowed for a contour plot that maps the laser response for a given range of external cavity lengths, which would have been of great use for comparison with the simulation results shown in chapter 3. The attempts to create such mappings were unsuccessful. The maps showed a lot of randomness that lead us to question the stability of the setup. To illustrate the instability of the setup the voltage supplied to the piezo actuators controlling the mirror positions were locked at arbitrary levels. The output of the spectrum analyzer was recorded for 2 hours. Figure 4.8 shows a contour plot of the captured peak mode of the laser for every read sample during that time.

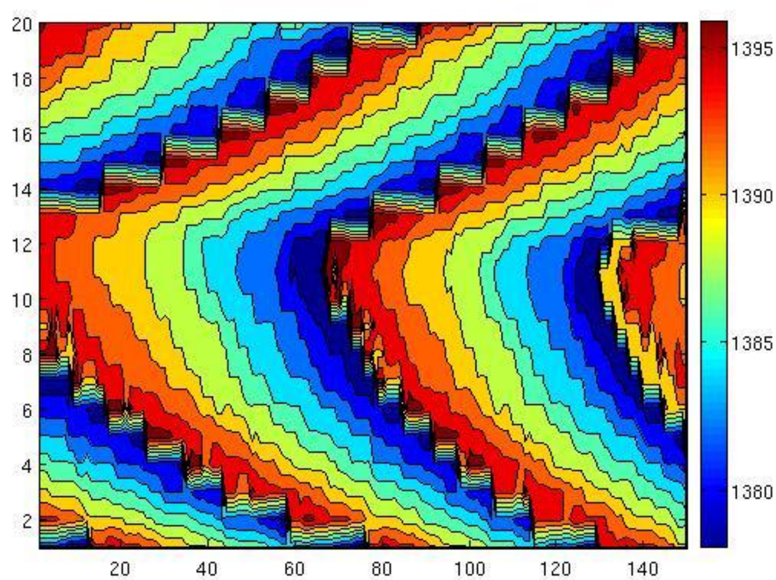

Figure 4.8: Dual Cavity Setup (Static Mirrors)

The plot shows that the mirror movements over time are too significant given the fact that it takes a few hours to execute the automated code described in the previous section. Thus it was not possible with the equipment available at hand to precisely map the output of the laser against known exact displacement in mirror positions.

Chapter 5

CONCLUSIONS

5.1 Conclusions

Various attempts of miniaturizing ECSLs were made since the beginning of this decade. These attempts utilized multiple micro-fabrication techniques to achieve that goal. Hinged vertical structures, fusion bonded SOI substrates and DRIE were amongst those techniques. The attempts also ranged from miniaturizing the simple 1-D geometry, which only requires basic linear microactuation, to complex grating based geometries that require rotational actuation.

The attempts had reasonable success in tuning a laser over a range of frequencies with decent side mode suppression. They, however, were for the most part bulky slow devices for the targeted scale. In the case of simple geometries the microactuators chosen were either overkill for the application or required to move the huge mirror structure. The complicated geometries did not lend themselves easily for miniaturization.

Simulating the model of a single cavity setup showed that this setup does not allow proper utilization of the full range available from a wide profile multimode laser. The external cavity has to be extended enough to allow for reasonable side mode suppression yielding a smaller tuning range. In contrast we showed by simulating the model of the Zhu/Cassidy dual cavity setup that the full tuning range can be maintained. The simulation was in agreement with their experimental results that continuous tuning through the various modes is not possible.

By giving the dual cavity setup an extra degree of freedom the simulations showed that it is possible to tune to any of the resonant frequencies available within the range. This can be realized by allowing both mirrors to be actuated.

In a hybrid large scale prototype we successfully demonstrated the claim. All frequencies available by the gain profile of the laser were achievable at decent side mode suppression. Due to limitations in the actuation accuracy of our setup it was not possible to tune to a particular mode at will in an automated fashion. The output was rather monitored at random variations in the two external cavity lengths over a prolonged period of time and the single mode lasing instances were mined from the data.

Table 5.1: Summary Table of MOEMS ECSL attempts in comparison to proposed setup

Group	**Geometry**	**Tuning Range**	**SMSR**	**Tuning Distance**	**Speed (switching time)**	**Tuning Voltage**	**Device Dimensions**
Nanyang University	1-D	16nm	>30dB	1µm 10-11µm		10 to 16V	2x1.5mm
		13.5nm	>13dB	1µm 66-70µm	2.5kHz (1ms)	2.5 to 18V	1.5x1mm
Imperial College	Littrow	20nm	>20dB	14µm		<50V	
Nanyang University		30.5nm	12-26dB			<30V	2x1.5mm
Imperial College	Littman	65nm	>22dB				5x5mm
Iolon Inc.		40nm	>55dB		(15ms)	-140 to 140V	5x5mm
This Work*	Dual Cavity	≥72nm	≥20dB	1µm 150-151 µm	>10MHz	<40V	0.3x0.2mm

* Projected and Calculated Values

Adopting a simple, yet effective, geometry as the one we propose in this work for a tunable ECSL enables further benefits from device miniaturization. The main areas of improvement are the overall device dimensions and the tuning speed. Our conservative calculations showed that a hybrid microfabricated device based on the dual cavity tuning geometry could be limited to 300µm x200µm x200µm and the tuning elements could resonate at 67MHz. Table 5.1 compares those calculations to other miniaturization attempts based on other geometries.

5.2 Future Research Recommendations

The natural progression of this work is to design a MEMS ECSL based on the dual cavity configuration described in this work. This could be followed by validating the design and conducting the microfabrication process. The device will then need to be thoroughly tested to verify its performance.

All MEMS devices discussed in this work including the design proposed are hybrid designs in which the microactuation are based on the MEMS fabrication techniques. This would also require us to research the multimode lasers that would fit in the proposed geometry to yield the best results.

A parallel effort to the hybrid designs could be directed towards growing a monolithic device using III/V materials to include the laser, the mirrors and the microactuator on one chip.

Appendix A

SIMULATION CODE (MATLAB M-SCRIPT)

A.1 Dual ECSL Simulation Function

```
%%%Dual External Cavity Laser Simulation Function%%%


function status=simulate(start1,finish1,start2,finish2)

%system properties

r1=0.32;
r2=0.32;
nd=3.4;
Ld=250*10^-6;
nc=1;
r3=0.32;
r4=0.004;
Go=7*10^-9;
gp=67.8;
lambda0=2*nd*Ld/1214;

%mode generation

m=1164:1264;
lambda=2*nd*Ld./m;
g=gp-((1/Go)*(lambda0-lambda)).^2;                          %Original laser gain profile
s=size(m');

%external cavities length generation based on the function input

Lc=start1*10^-6:0.01*10^-6:finish1*10^-6;
Lc2=start2*10^-6:0.01*10^-6:finish2*10^-6;

%applying the effective reflectivity model to find the wavelength with the highest gain
%value and the side mode suppression for every generated Lc and Lc2 values

for nun=1:size(Lc2')
    for n=1:size(Lc')
        for n2=1:s(1)
            reff1=(r2+r3*exp(-4*pi*Lc(n)*nc*j/lambda(n2)))/(1+r2*r3*exp(-
4*pi*Lc(n)*nc*j/lambda(n2)));
            reff2=(r1+r4*exp(-4*pi*Lc2(nun)*nc*j/lambda(n2)))/(1+r1*r4*exp(-
4*pi*Lc2(nun)*nc*j/lambda(n2)));
            alpha(n2)=(1/(100*Ld))*log(1/(abs(reff2)*abs(reff1)));
        end
        netgain=g-alpha;
        [y I]=max(netgain);
        tuning(nun,n)=lambda(I);
        netgain(I)=-1000000000;
        [x H]=max(netgain);
        deltagain(nun,n)=abs(y-x);
    end
end

%results exported to a data file for analysis purposes

fileout1=['tuning',num2str(start2),'_',num2str(start1),'.dat'];
fileout2=['sms',num2str(start2),'_',num2str(start1),'.dat'];

%results used to generate output contour plots
```

```
contourf(tuning);
figure;
contourf(deltagain);
status=0;

%%%End of Code%%%
```

A.2 Full Range Simulation

```
%%%50umx250um simulation%%%

for i=1:25
    for j=1:50
        simulate(2*i,2*(i+1),5*j,5*(j+1));%The simulation is composed out of 2umx5um
    end                                            %units
end
%%%End of Code%%%
```

A.3 Simulation Analysis

```
%%%Analyze The Simulated Data Files%%%

for j=1:50                                        %Open every 2umx5um tuning and sms data file
    for i=1:25
        filein1=['tuning',num2str(5*j),'_',num2str(2*i),'.dat'];
        filein2=['sms',num2str(5*j),'_',num2str(2*i),'.dat'];
        A=dlmread(filein1);                                  %Store the wavelength data in matrix A
        B=dlmread(filein2);                                         %Store the sms data in matrix B
        range(i,j)=(max(max(A))-min(min(A)))/1e-9;%Find the tuning range and convert to
                                                                      %nm
        sms(i,j)=max(max(B));                                           %Find the peak sms value
    end
end

%%%End of Code%%%
```

Appendix B

Device Design Side Calculations

B.1 Force per Unit Length Acting On Mirror

The electrostatic force acting on the mirror can be calculated as a function of the capacitance, the voltage applied and the air gap to the mirror according to equation (B.1).

$$F = \frac{CV^2}{2\mathrm{d}} \tag{B.1}$$

The capacitance in equation (B.1) in the case of an air gap can be found by applying equation (B.2).

$$C = \frac{\varepsilon_o AV^2}{d} \tag{B.2}$$

By substituting (B.1) into (B.2) we get equation (B.3).

$$F = \frac{\varepsilon_o AV^2}{2\mathrm{d}^2} \tag{B.3}$$

It then follows that the force acting on a unit length of the mirror is defined by equation (B.4).

$$\omega_l = \frac{F}{l} = \frac{\varepsilon_o hV^2}{2\mathrm{d}^2} \tag{B.4}$$

B.2 Voltage Needed to Generate Desired Deflection

If we model the system to that of a beam attached on both sides the maximum deflection allowed for that beam as a function of the strain of its material, its length and the force per unit length acting along the beam can be described by equation (B.5).

$$y_{max} = \frac{-\omega_l l^4}{384 E_{si} I} \tag{B.5}$$

By substituting in equation (B.5) from our findings in equation (B.4) we arrive at equation (B.6) which shows the voltage required to cause a structure of that size and geometry to deflect to a particular maximum deflection value.

$$V = \sqrt{\frac{2\mathrm{d}^2 E_{si} I \mid y_{max} \mid}{\varepsilon_o h l^4}} \tag{B.6}$$

B.3 Natural Frequency of Mirror

Using the same model we can find the natural frequency of resonance for that structure as a function of its mass, the mode of resonance, its geometry and the material it is made from as described in equation (B.7).

$$f_n = \frac{k_n}{2\pi} \sqrt{\frac{E_{si} I}{m l^3}} \tag{B.7}$$

The mass of the mirror can be simply calculated from equation (B.8).

$$m = \rho_{si} V_{mirror} \tag{B.8}$$

B.4 Calculation Code (Python Script)

```
from math import sqrt

#System Parameters

l=150*10**(-6)
h=60*10**(-6)
t=2*10**(-6)
d=5*10**(-6)
ymax=1*10**(-6)

#Constants

E_si=190*10**(9)
rho_si=2300
epsilon_o=8.8542*10**(-12)
kn=22.4
g=9.8
pi=3.14159

#Calculations

I=(h*(t**3))/(12)
V=sqrt((2*(d**2)*E_si*I*ymax)/(epsilon_o*h*(l**4)))
m=rho_si*l*t*h
fn=(kn/(2*pi))*sqrt((E_si*I)/(m*(l**3)))

#Outputs

print "V=%f" %V
print "fn=%f" %
```

References

[1] A. Q. Liu, X. M. Zhang, V. M. Murukeshan, C. Lu, and T. H. Cheng, "Micromachined wavelength tunable laser with an extended feedback model," IEEE Journal of Selected Topics in Quantum Electronics, vol. 8, no. 1, pp. 73–79, 2002.

[2] R. R. Syms and A. Lohmann, "MOEMS tuning element for a Littrow external cavity laser," Journal of Microelectromechanical Systems, vol. 12, no. 6, pp. 921–928, 2003.

[3] A. Q. Liu, X. M. Zhang, J. Li, and C. Lu, "Single-/multi-mode tunable lasers using MEMS mirror and grating," Sensors & Actuators: A. Physical, vol. 108, no. 1, pp. 49–54, 2003.

[4] C. Ye, Tunable external cavity diode lasers. World Scientific, 2004.

[5] L. A. Coldren, G. A. Fish, Y. Akulova, J. S. Barton, L. Johansson, and C. W. Coldren, "Tunable semiconductor lasers: A tutorial," Journal of Lightwave Technology, vol. 22, no. 1, p. 193, 2004.

[6] L. S. Rothman et al., "The HITRAN molecular spectroscopic database: edition of 2000 including updates through 2001," Journal of Quantitative Spectroscopy and Radiative Transfer, vol. 82, no. 1, pp. 5–44, 2003.

[7] P. W. Werle, P. Mazzinghi, F. D'Amato, M. De Rosa, K. Maurer, and F. Slemr, "Signal processing and calibration procedures for in situ diode-laser absorption spectroscopy," Spectrochimica Acta Part A: Molecular and Biomolecular Spectroscopy, vol. 60, no. 8, pp. 1685–1705, 2004.

[8] X. Zhu, "Tunable Diode Lasers and their Applications in Gas and Liquid Detection," Ph.D. Thesis, McMaster University, 1997.

[9] L. Coldren and T. Koch, "External-cavity laser design," Lightwave Technology, Journal of, vol. 2, no. 6, pp. 1045–1051, 1984.

[10] N. Gade and J. Osmundsen, “Gain measurements on semiconductor lasers by optical feedback from an external grating cavity,” Quantum Electronics, IEEE Journal of, vol. 19, no. 8, pp. 1238–1242, 2002.

[11] W. R. Trutna Jr and L. F. Stokes, “Continuously tuned external cavity semiconductor laser,” Lightwave Technology, Journal of, vol. 11, no. 8, pp. 1279–1286, 1993.

[12] R. A. Conant et al., “A raster-scanning full-motion video display using polysilicon micromachined mirrors,” Sensors and Actuators A: Physical, vol. 83, no. 1, pp. 291–296, 2000.

[13] J. Wen, X. D. Hoa, A. G. Kirk, and D. A. Lowther, “Analysis of the performance of a MEMS micromirror,” Magnetics, IEEE Transactions on, vol. 40, no. 2, pp. 1410–1413, 2004.

[14] P. O. Vaccaro, K. Kubota, and T. Aida, “Strain-driven self-positioning of micromachined structures,” Applied Physics Letters, vol. 78, no. 19, p. 2852, 2001.

[15] J. Plummer, M. D. Deal, and P. B. Griffin, Silicon VLSI Technology. Pearson Higher Education & Professional Group, 2000.

[16] K. S. J. Pister, M. W. Judy, and others, “Microfabricated hinges,” Sensors and Actuators A: Physical, vol. 33, no. 3, pp. 249–256, 1992.

[17] J. R. Reid, V. M. Bright, and J. H. Comtois, “Automated assembly of flip-up micromirrors,” in Solid State Sensors and Actuators, 1997. TRANSDUCERS'97 Chicago., 1997 International Conference on, vol. 1, pp. 347–350, 2002.

[18] A. A. Ayon, S. Nagle, L. Frechette, A. Epstein, and M. A. Schmidt, “Tailoring etch directionality in a deep reactive ion etching tool,” Journal of Vacuum Science & Technology B: Microelectronics and Nanometer Structures, vol. 18, p. 1412, 2000.

[19] K. S. Chen, A. A. Ayón, X. Zhang, and S. M. Spearing, “Effect of process parameters on the surface morphology and mechanical performance of silicon structures after deep reactive ion etching (DRIE),” Journal of Microelectromechanical Systems, vol. 11, no. 3, pp. 264–275, 2002.

[20] C. Marxer et al., “Vertical mirrors fabricated by deep reactive ion etching forfiber-optic switching applications,” Microelectromechanical Systems, Journal of, vol. 6, no. 3, pp. 277–285, 1997.

[21] X. M. Zhang, A. Q. Liu, V. M. Murukeshan, and F. Chollet, “Integrated micromachined tunable lasers for all optical network (AON) applications,” Sensors and Actuators A: Physical, vol. 97, pp. 54–60, 2002.

[22] X. M. Zhang, A. Q. Liu, D. Y. Tang, and C. Lu, “Discrete wavelength tunable laser using microelectromechanical systems technology,” Applied Physics Letters, vol. 84, p. 329, 2004.

[23] R. R. Syms and A. Lohmann, “MOEMS tuning element for a Littrow external cavity laser,” Microelectromechanical Systems, Journal of, vol. 12, no. 6, pp. 921–928, 2004.

[24] X. M. Zhang, A. Q. Liu, C. Lu, and D. Y. Tang, “Continuous wavelength tuning in micromachined Littrow external-cavity lasers,” Quantum Electronics, IEEE Journal of, vol. 41, no. 2, pp. 187–197, 2005.

[25] W. Huang, R. R. A. Syms, J. Stagg, and A. Lohmann, “Precision MEMS flexure mount for a Littman tunable external cavity laser,” in Science, Measurement and Technology, IEE Proceedings-, vol. 151, pp. 67–75, 2004.

[26] J. D. Berger, Y. Zhang, J. D. Grade, H. Lee, S. Hrinya, and H. Jerman, “Widely tunable external cavity diode laser based on a MEMS electrostatic rotary actuator,” in Optical Fiber Communication Conference and Exhibit, 2001. OFC 2001, vol. 2, 2005.

[27] T. P. Lee, C. Burrus, J. Copeland, A. Dentai, and D. Marcuse, “Short-cavity InGaAsP injection lasers: Dependence of mode spectra and single-longitudinal-mode power on cavity length,” Quantum Electronics, IEEE Journal of, vol. 18, no. 7, pp. 1101–1113, 2002.

[28] M. G. Littman and H. J. Metcalf, “Spectrally narrow pulsed dye laser without beam expander,” Applied Optics, vol. 17, no. 14, pp. 2224–2227, 1978.

[29] X. Zhu and D. T. Cassidy, "Liquid detection with InGaAsP semiconductor lasers having multiple short external cavities," Applied Optics, vol. 35, no. 24, pp. 4689–4693, 1996.